Testing non-destructive spectrometric methods for the identification and distinction of archaeological pine wood tar and birch bark tar

Despotopoulou, Myrto; Langejans, Geeske H.J.; Hendrikx, Ruud W.A.; Joosten, Ineke; Nijemeisland, Marlies; Poulis, Johannes A.; Kozowyk, Paul R.B.

DOI
10.1016/j.jasrep.2024.104571

Publication date
2024

Document Version
Final published version

Published in
Journal of Archaeological Science: Reports

Journal of Archaeological Science: Reports 56 (2024) 104571

Contents lists available at ScienceDirect

Journal of Archaeological Science: Reports

journal homepage: www.elsevier.com/locate/jasrep

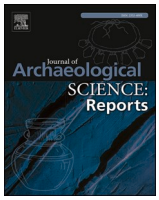

Testing non-destructive spectrometric methods for the identification and distinction of archaeological pine wood tar and birch bark tar

Myrto Despotopoulou [a], Geeske H.J. Langejans [a,d], Ruud W.A. Hendrikx [a], Ineke Joosten [b], Marlies Nijemeisland [c], Johannes A. Poulis [c], Paul R.B. Kozowyk [a,*]

[a] Faculty of Mechanical Engineering, Delft University of Technology, Mekelweg 2, 2628 CD Delft, the Netherlands
[b] Cultural Heritage Agency of the Netherlands (RCE), PO Box 1600, 3800 BP Amersfoort, the Netherlands
[c] Faculty of Aerospace Engineering, Delft University of Technology, Kluyverweg 1, 2629 HS, Delft, the Netherlands
[d] Centre for Anthropological Research, University of Johannesburg, Palaeo-Research Institute, House 10, Humanities Research Village, APB, Auckland Park 2006, South Africa

ARTICLE INFO

Keywords:
Adhesives
Pine wood tar
Birch bark tar
Non-destructive
Scanning Electron Microscopy – Energy Dispersive X-ray Spectroscopy (SEM-EDS)
Fourier-Transform Infrared (FTIR) microspectroscopy
X-ray Diffraction (XRD)

ABSTRACT

Archaeological findings prove the appearance and use of birch bark tar since the Middle Palaeolithic. The production and use of birch bark tar and pine wood tar has overlapped since at least the late Neolithic, but probably for much longer. The reliable chemical identification of such archaeological tar residues can offer valuable insights into, for example, ancient technical complexity, trade and culture. In this context, the scarcity of these mainly organic residue findings in the archaeological record bears the need for non-destructive analytical tools. However, there is currently no systematic proposed way for this purpose. We aim here to verify the organic nature and test the reliability of the identification of archaeological pine wood tar and birch bark tar with a combination of SEM-EDS, FTIR microspectroscopy in reflectance mode and XRD. We examined a set of experimental adhesive replicas of pine tar and birch tar in pristine form, but also after a three-year-long weathering experiment. Additionally, we studied a set of archaeological samples, consisting of Mesolithic bone/antler points with adhering hafting residues, form the Dutch North Sea. This research shows that degradation negatively influences the reliable verification and identification of the organic residue constituents significantly. SEM-EDS as a starting point of analysis verifies the residue's organic nature, but it cannot be used to identify birch or pine tar. XRD can identify crystalline additives in the adhesive mixture, like ochre and wax, as well as phases related to the artefact's environment of burial and provenance. Micro-FTIR is also capable of verifying the organic matter of the residue constituents. The differentiation of birch and pine tars is hindered by vibrational modes occurring in neighbouring wavenumbers for both tars, and by the limited research on degradation markers indicative of thermal treatment to prove tar production. Until reference collections also account for degradation and include a wide variety of adhesives, results of FTIR collected in reflectance mode are best treated with some caution.

1. Introduction

The use of adhesive materials in prehistory started with organic products naturally exhibiting tacky properties, like tree resin exudates or starchy foods and proceeded to include more complex adhesives, necessitating human-induced fabrication processes (Langejans et al., 2022; Regert et al., 2003). A characteristic example of such adhesives are pine tar and birch tar, products of destructive distillation of biomass.

The earliest currently known adhesive finding corresponds to birch bark tar with a minimum age of 191,000 years old (Mazza et al., 2006). It is followed by natural bitumen residues dated to around 70,000 years ago (Boëda et al., 2008). Presently, the oldest evidence of conifer resin has an age of about 65,000 to 40,000 years ago (Degano et al., 2019). The earliest finding of pine tar is attributed to a Late Neolithic site from about 3,200–3,000 years ago. However, the existence of evidence for pine tar use in Europe from the Upper Palaeolithic and Mesolithic is a

* Corresponding author.
E-mail addresses: myrtodesp@gmail.com (M. Despotopoulou), g.langejans@tudelft.nl (G.H.J. Langejans), r.w.a.hendrikx@tudelft.nl (R.W.A. Hendrikx), i.joosten@cultureelerfgoed.nl (I. Joosten), m.nijemeisland@bb.leidenuniv.nl (M. Nijemeisland), j.a.poulis@tudelft.nl (J.A. Poulis), p.r.b.kozowyk@tudelft.nl (P.R.B. Kozowyk).

https://doi.org/10.1016/j.jasrep.2024.104571
Received 16 March 2023; Received in revised form 22 April 2024; Accepted 29 April 2024
Available online 10 May 2024

possibility (Langejans et al., 2024).

While it is not yet clear when it was first discovered and manufactured, pine tar has been used for a variety of applications such as hafting, waterproofing (Rageot et al., 2016) and sealing (Heron and Evershed, 1993). Birch bark tar also has a wide range of known applications, such as hafting (Mazza et al., 2006), coating (Rageot et al., 2021), repairing of ceramic (Urem-Kotsou et al., 2002) and metal (Courel et al., 2018) objects, and even as a (medicinal) chewing gum (Aveling and Heron, 1999).

The choice among different adhesives for prehistoric people is linked to raw material availability, and also to technical knowledge (Langejans et al., 2022). Moreover, adhesive production can be an indication of the technological and by proxy possibly the cognitive complexity of ancient hominins like Neanderthals (Fajardo et al., 2023; Wragg Sykes, 2015). Additionally, it can reveal the socio-economic networks rising from trading among past civilisations (Connan and Van de Velde, 2010; Kristiansen and Suchowska-Ducke, 2022; Rageot et al., 2021). Although the occurrence of pine and birch trees overlaps in Europe for the best part of the Pleistocene (Bigga et al., 2014), the fabrication and use of their tars has only overlapped in the archaeological record since about the 4th millennium BCE (Mitikidou et al., 2008). A possible explanation for the lack of pine wood tar in the Palaeolithic, stems from indications that birch bark tar appears to preserve better than pine tar and pine resin (Kozowyk et al., 2020).

In this context, it is essential to enable the identification and distinction between the two types of tars, through reliable chemical analysis methods. However, the identification of mainly organic adhesive remnants is challenging due to their susceptibility to natural decay. Any archaeological findings, which mostly come in the form of microscopic residues, are thus rare and valuable (Kozowyk et al., 2017; Monnier et al., 2013; Regert et al., 2003). The most reliable and widespread identification method for archaeological adhesives is Gas Chromatography – Mass Spectrometry (GC-MS) (Chapters et al., 1993; Heron and Evershed, 1993; Rageot et al., 2019; Regert, 2004). Despite its reliability, GC-MS is invasive and destructive; a problem when analysing these scarce archaeological materials.

A variety of non-destructive techniques have been implemented for the characterisation of archaeological adhesive mixtures. These techniques were often used in various combinations with other destructive and non-destructive methods of analysis. Resins and waxes have been analysed with Raman spectroscopy (Edwards et al., 1996), while bitumen residues on three Palaeolithic stone tools from Hummal, Syria were studied with Raman microspectroscopy, combined with FTIR microspectroscopy, EDS and XRD (Monnier et al., 2013). Organic residues on Roman ceramic vessels late Roman-Egyptian adhesives were characterised with a combination of GC-MS and FTIR (Colombini et al., 2005; Ribechini et al., 2009). However, no systematic approach was established or tested for the study of these archaeological adhesive residues in a completely non-destructive manner.

Here, we aim to tackle this research gap by testing the ability of non-destructive analytical methods to identify and distinguish pine tar and birch tar in archaeological adhesive mixtures. In this context, it is important to account for the effects of morphological and chemical degradation. For this purpose, we analysed a set of experimental pine tar and birch tar samples, in pristine and weathered form. Additionally, we studied an assemblage of archaeological artefacts with residues characterised by GC-MS as birch bark tar. A combination of scanning electron microscopy – energy dispersive X-ray spectroscopy (SEM-EDS), Fourier-transform infrared microspectroscopy (micro-FTIR) and X-ray diffraction (XRD) was used for this scope.

2. Materials and methods

2.1. Materials

Pine tar is produced by the destructive distillation of pine tree wood of the Pinaceae family. It predominantly contains tricyclic diterpenoid acids with abietane, pimarene and isopimarane skeletons. Abietic, pimaric and isopimaric acids are biomarkers of fresh pine resin, and these are also contained in pine tar as native biomarkers. Dehydroabietic, dehydro-7-dehydroabietic and 7-oxodehydroabietic acids result from oxidation or aromatisation processes of the native markers, either caused by ageing or anthropogenic introduction of heat (Regert, 2004). It is thus difficult to deduce whether the presence of degradation markers is a result of natural decay of pine resin or caused by anthropogenic heat input to produce tar. The degradation markers that are reliable markers of pine tar are retene, methyl dehydroabietate and 1,7-dimethylphenanthrene; these are generally considered as products of the human-induced distillation process (Rageot et al., 2016).

Birch tar is produced by the pyrolysis or destructive distillation of birch (*Betula* sp.) tree bark (Rageot et al., 2019). Birch bark tar consists of pentacyclic triterpenoids of the lupane family. Fresh birch bark mainly consists of the following triterpenoid biomarkers: betulin, lupeol, lupenone, betulone, erythrodiol and betulinic acid (Rageot et al., 2021; Regert, 2004). Degradation markers result from the thermal treatment for tar production or because of natural decay (Chapters et al., 1993; Rageot et al., 2021, 2016). Lupenone and betulone pre-exist naturally in birch bark, but their proportion may increase during tar production, because of the oxidation of lupeol and betulin, respectively (Regert, 2004).

The effect of natural decay is a decisive factor for the study of archaeological artefacts, due to the degradation of the materials' biomarkers. The consideration of this effect is of the highest importance for applying a non-destructive analytical methodology to archaeological artefacts. Therefore, we studied three sample categories: two types of experimental samples, pristine and weathered adhesive replicas, as well as a set of archaeological samples (Table 1).

2.1.1. Experimental samples

The experimental pine wood tar and birch bark tar replicas (Fig. 1a-d) for both types of experimental samples were sourced from a previous experiment (Kozowyk et al., 2020). The weathered samples (Fig. 1b and c) originate from an experiment in which the two tars were replicated and used to haft flint flakes in 10-mm diameter pine wood dowels. The hafted flint flakes were then left to weather in three-year-long field experiment. The objects with adhesives were buried at the Dutch conservation area, the Horsterwold (Flevoland province) in the Netherlands. The hafted flint flakes were retrieved after the burial, softly cleaned with a paintbrush and water to remove the sediment excess. The weathered material was analysed *in situ*, on the tools.

The pristine experimental tars contain the same adhesive ingredients as the ones of the weathered samples. These samples were melted in aluminium cups with the use of a conventional electric hot plate. While in a molten state, a small quantity of each adhesive was poured onto a flat aluminium sample bar (Fig. 1a), and covered in aluminium foil to protect it until analysis.

Table 1
Sample list.

Category	Adhesive / Origin	Description	Sample ID
Experimental	Pine wood tar	Pristine	NDP01
		Weathered	Hor3189
	Birch bark tar	Pristine	NDP02
		Weathered	Hor3225
Archaeological	Bone points from the Dutch North Sea	Barbed point	NSM03
		Barbed point	NSM10
		Point/awl	NSM15
		Barbed point	NSM16
		Barbed point	NSM18
		Barbed point	NSM28
		Loose residues from NSM18	NSM31

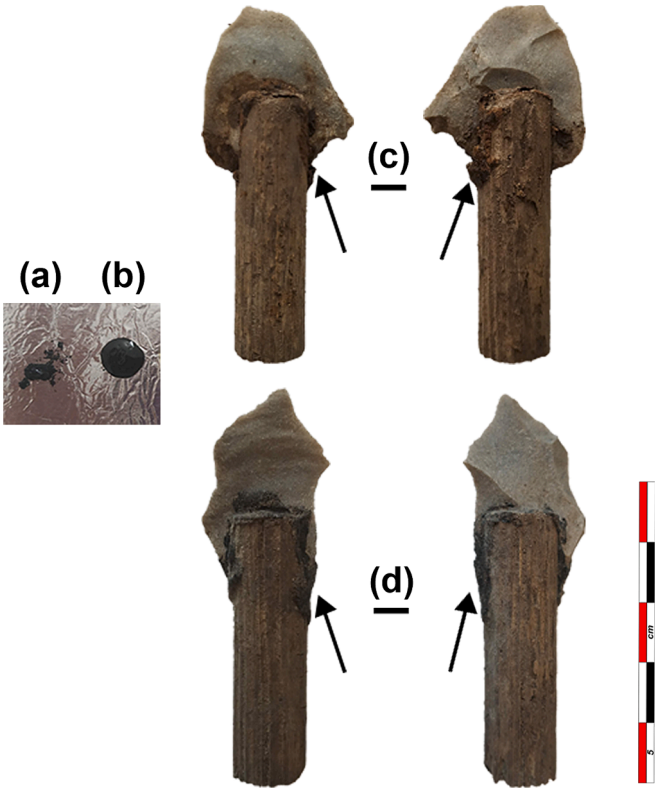

Fig. 1. (a) Pristine experimental pine wood tar (NDP01), (b) pristine experimental birch bark tar (NDP02), (c) weathered experimental pine wood tar (Hor3189), (c) weathered experimental birch bark tar (Hor3201). Arrows indicate the preserved hafting adhesives. The scale bar indicates 5 cm.

2.1.2. Archaeological samples

The archaeological samples consist of a set of six Mesolithic bone points recovered from redeposited sediments on the Dutch shoreline (Table 1, Fig. 2). These sediments were dredged from the North Sea and used to consolidate the coastline (Amkreutz and Spithoven, 2019). Both archaeologists and amateurs have been collecting them from such beaches. The points exhibit macroscopic and microscopic evidence of hafting, discolouration, and residues believed to be of adhesive nature. All the bone points in this study were on loan from private collections, apart from NSM28, which was on loan from the Rijksmuseum van Oudheden (Dutch National Museum of Antiquities) in Leiden. The points were soaked in distilled water several times by the custodians, as this is a standard practice for objects retrieved form marine environments. The discolourations and residues were analysed *in situ*, on the tools. NSM31, which is the loose residue of NSM18, was the only exception.

2.2. Characterisation methods

A set of three non-destructive characterisation methods were applied in the identification of the adhesive mixture constituents: Scanning Electron Microscopy – Energy Dispersive X-ray Spectroscopy (SEM-EDS), Fourier-Transform Infrared microspectroscopy (micro-FTIR) and X-ray Diffraction (XRD). Two locations on the pristine experimental samples were analysed with SEM-EDS and micro-FTIR, while one reading was collected with XRD. For the weathered experimental samples, two readings were performed on the residue. Additional readings were collected from the flint and the wood, providing a comparison of the tool surface with no visible residues. Two residue readings were collected from the residue/discolouration area of each archaeological samples as well, along with one bone reading that also serves as the background reading. Exceptions to this rule arose occasionally, due to sample particularities and availability. In total, we conducted 75 measurements (Table S1). Only the measurements corresponding to the residue or discolouration areas of interest are presented here. The measurements collected from the substrate materials (flint, wood or bone) can be found in the supplementary material.

2.2.1. Scanning electron microscopy – Energy Dispersive X-ray spectroscopy (SEM-EDS)

Because the samples are porous, fragile and cannot be coated, we used an environmental (ESEM) or low-vacuum (LVSEM) SEM microscope (Adriaens and Dowsett, 2004; Ominami, 2018). The JEOL JSM-IT700HR InTouchScope™ scanning electron microscope, with a JED-2300-Fully integrated EDS system (100 mm^2 SDD) was used for the SEM-EDS analysis in this project. The measurement parameters are summarised in Table 2. The samples were stabilised on the sample plate with double-sided carbon tape and aluminium stubs. The peaks of EDS spectra were automatically assigned to the corresponding elements through the software incorporated in the system controlling the equipment.

2.2.2. Fourier-transform infrared microspectroscopy (micro-FTIR)

Coupling an FTIR spectrometer with an optical microscope for non-destructive characterisation is particularly useful for the analysis of very small-scale samples or very small components in heterogeneous samples. The beam size ranges from 20 to 100 μm with the standard radiation source.

A Perkin Elmer Spotlight 400 FTIR microscope, coupled with a Perkin Elmer Frontier FT-IR spectrometer were used for the micro-FTIR analysis. Spectrum IR was used for equipment control and data evaluation. The measurements were performed in diffusive reflectance mode to secure their non-destructive nature, with a resolution of 4 cm^{-1}, 16 accumulations per measurement, a spot size of 100x100 μm, in the wavelength range of 4000–600 cm^{-1}. The weathered experimental and the archaeological samples were positioned on the sample stage and stabilized with the use of Blu tac, covered with a small piece of latex laboratory gloves, to prevent the contamination of the samples by the putty material.

Only the peak positions assigned to vibrational modes of the compounds of interest (pine or birch tar) are highlighted in the spectra presented in this paper.

2.2.3. X-ray diffraction (XRD)

A Bruker D8 Discover diffractometer and Eiger-2 500 k 2D-detector were used for the X-ray diffraction analysis in this project. Cu Kα radiation and an Incoatec 1μS microfocus tube were used for the measurements at 50 kV, 1000 μA. The equipment includes a UBC 1.0 mm collimator, scatter screen and a UMC 1516 sample stage. The software for equipment control and data evaluation was the Bruker DiffracSuite. EVA vs 5.2. The measurement parameters for each sample category are summarised in Table 3. The measured XRD patterns were subject to background subtraction and small displacement correction. The coloured bars in the resulting patterns provide the peak positions and intensities of the possibly present crystalline phases, using the ICDD pdf4 database.

2.3. Predictions

Based on the characteristics of our set of samples, in combination with the principle and limitations of the applied analytical methods, we can have some specific expectations for the results of this non-destructive analysis.

Firstly, the thickness of the adhesive layer is expected to affect the detected signal and, as a result, the identification process. When the samples are analysed *in situ*, the contribution of the underlying substrate to the signal can be particularly strong where the layer is thin. This might interfere with the signal of the residue and hinder identification. Our pristine experimental samples are deposited in much thicker layers,

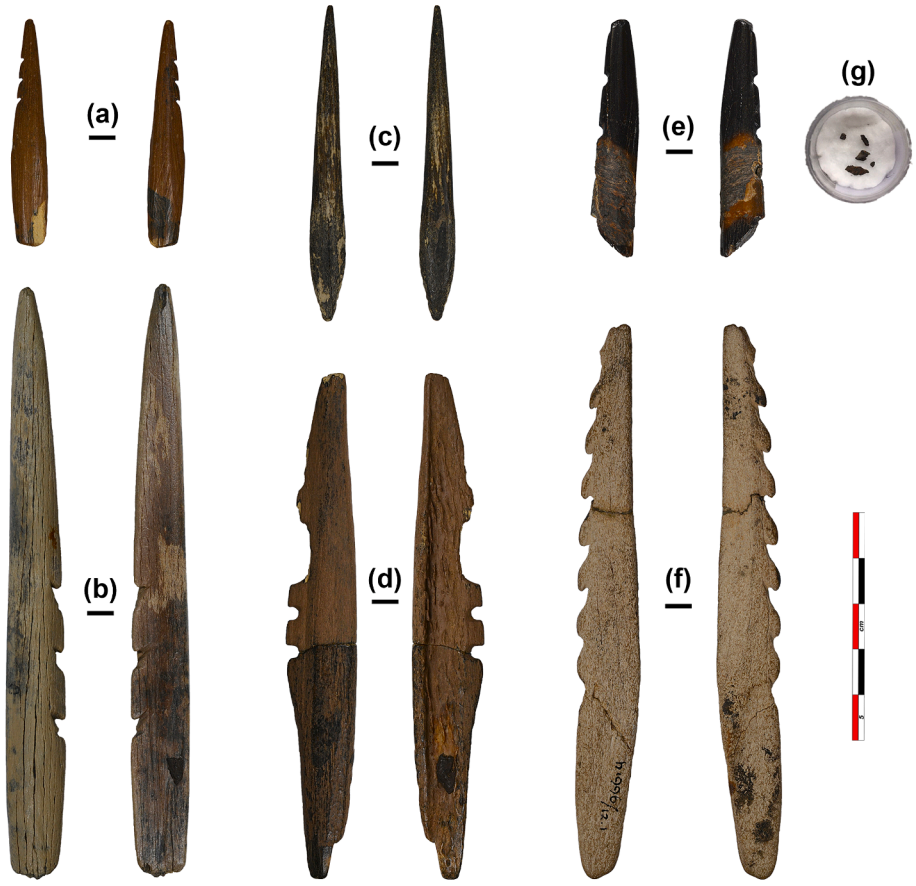

Fig. 2. Archaeological samples, bone points from the Dutch North Sea, photos of both sides. (a) NSM03, (b) NSM16, (c) NSM15, (d) NSM10, (e) NSM18, (f) NSM28 and (e) NSM31 (loose residues form NSM18). The scale bar indicates 5 cm.

Table 2
SEM-EDS measurement parameters for each sample category.

Samples		Accelerating voltage (kV)	Working distance (mm)	Vacuum (Pa)
Experimental	Pristine	20	7.8–9.9	30
	Weathered	20	9.6–14.5	22–44
Archaeological		5, 10, 20	8.9–11.8	70

Table 3
XRD measurement parameters for each sample category.

Samples		θ-2θ range (°2θ)	2θ step (°)	Step time (s)	Comments
Experimental	Pristine	5–60	0.04	2	samples fixed on standard sample table
	Weathered	10–70	0.02		
Archaeological		10–70	0.02		samples lying on a Si510 zero-background wafer, on standard sample table

compared to the weathered experimental samples. The residues on the bone points under examination here, vary in their thickness as well. In general, most archaeological residues are expected to be thinner than the thickness of our pristine samples, due to environmental exposure or decay. In addition, the thickness of their adhesive layers is expected to vary across the tool surface. As a result, archaeological samples bearing adhesive residues are likely to be affected by this issue, depending on the location of analysis. It is therefore important to collect clean readings from the bare substrates underlying the adhesives, to be able to extrapolate their signal features. For our weathered experimental samples, we anticipate contribution from the wood dowel and the quartz (SiO_2) of the flint. The results of the archaeological bone points are expected to include signal from the bone's organic and inorganic components, namely collagen and hydroxyapatite ($Ca_5(PO_4)_3(OH)$), respectively.

Furthermore, the environment of the artefacts' weathering will most probably affect the measurement results. In our case, this is mostly the effect of sediment remains from the site of burial. Quartz (SiO_2), calcite ($CaCO_3$) and clay, mainly kaolinite, are very common in archaeological sediments (Weiner, 2010) and we expect to detect them in the collected spectra. As far as our archaeological samples are concerned, we also anticipate contribution from the marine weathering environment. This can be in the form of salt remnants. However, it is also worth mentioning that the degradation of organic matter in anoxic marine environments by sulphate-reducing bacteria can lead to the production of iron sulphides, such as pyrite (FeS_2) (Schippers and Jorgensen, 2002). Given the provenance of this set of bone points, iron sulphides detected in the spectra, as the result of adhesive residue degradation, can be an indirect indication for the residue's organic nature.

3. Results

3.1. SEM-EDS

3.1.1. Pristine experimental tars

The SEM-EDS analysis of the pristine experimental tars clearly

verifies the organic nature of both materials, through significantly strong carbon (C) peaks in the EDS spectra (Fig. 3a-d). Weak aluminium (Al) peaks also emerge in the spectra as a contribution from the aluminium foil lying under the deposited adhesive material. The backscattered images show a sharp difference in the surface morphology of the two pristine experimental tars. The surface of pristine birch tar (Fig. 3g-h) appears as quite even and homogeneous, with only a few contamination particles. On the contrary, the surface of pristine pine tar (Fig. 3g-h) seems much more irregular with a significantly higher number of overlaying contamination particles. Based on this observation, we consider the iron (Fe) detected in the EDS spectra of pristine pine tar (Fig. 3a-b) as the result of contamination from an iron oxide.

3.1.2. Weathered experimental tars

The organic nature of tars is very easily verified through the EDS analysis in their weathered state too (Fig. 4a-d). The particularly strong carbon (C) peaks in Fig. 4b-d prove that the three-year long weathering of the tars does not affect the verification of organic.

Sediment contamination is apparent through the appearance of silicon (Si), calcium (Ca) and aluminium (Al) in both weathered samples. While the detection of silicon could also result from the flint substrate, the backscattered images (Fig. 4e-g), show a strong effect from surface contamination from the adhering sediment. As a result, it is most likely that the silicon contribution is due to overlaying sediment particles. The EDS spectra of Fig. 4a show a sharp difference in elemental composition compared to every other weathered tar spectrum. The organic content (C) is significantly lower, and many elements such as iron (Fe), aluminium (Al), phosphorous (P), sulphur (S), calcium (Ca), magnesium (Mg) and potassium (K) have a stronger contribution. The granular morphology of the corresponding backscattered (BSE) image in Fig. 4e suggests that these spectra were probably collected from a post-depositional sediment particle overlaying the adhesive.

3.1.3. Archaeological tar

The interpretation of the SEM-EDS results becomes more complicated for the aged archaeological samples (Figs. 5, 6, 7, 8). Out of the four points that were studied with this method, only the residues of NSM10 (Fig. 6b) and NSM16 (Fig. 8) generated carbon (C) peaks sufficiently strong to verify them as organic. The discolourations on NSM03 and NSM15 were not verified as organic through the EDS analysis, based on the intensity of the carbon peaks. Sulphur (S) is detected in the spectra of NSM10 (Fig. 6a-b) and NSM15 (Fig. 7a). In the latter, iron (Fe) is detected too. Since the SEM-EDS analysis produced no indications of organic content for NSM03 and NSM15, these bone points will not be further discussed with the other methods. The corresponding micro-FTIR and XRD results can be found in the supplementary information. The spectra collected from the residue/discolouration areas of all four points demonstrate a strong contribution of calcium (Ca) and phosphorus (P), probably originating from the underlying bone's hydroxyapatite ($Ca_5(PO_4)_3(OH)$). Low sodium (Na), chlorine (Cl), magnesium (Mg) and aluminium (Al) content might originate from contamination by the sediment or during handling of the artefacts.

3.2. Micro-FTIR spectroscopy

The micro-FTIR spectra of pristine experimental, weathered experimental and archaeological samples are illustrated in Fig. 9, Fig. 10 and Fig. 11, respectively (full spectra in Figure S4-S6). The infrared spectrum region between 4000 cm^{-1} and 2000 cm^{-1} range is not included in our analysis, as it corresponds to stretching O-H vibrations of hydrogen bonded hydroxyl groups and stretching C-H vibrations of the methylene ($-CH_2$) and methyl ($-CH_3$) groups. They are thus not useful for the distinction between the two tars. Only the most indicative part of the spectrum, which lies between 2000 cm^{-1} and 800 cm^{-1}, is included.

In the quest to identify the materials under examination, their peaks are assigned, when possible to those of pine tar (Font et al., 2007; Martín-Ramos et al., 2018; Monnier, 2017) and birch tar (Cîntă-Pînzaru et al., 2012; Vahur et al., 2016) from the literature. Among the previous research, there are few assignments of the bands in their spectra to particular markers of each type of tar.

Reflectance infrared spectroscopy is useful as a non-destructive, non-invasive, non-contact method for testing solid surfaces. Three different phenomena are observed in the FTIR spectra: diffusive reflection, specular reflection and a large part of absorption of the IR light by the sample. However, the interpretation of the data can be challenging due to the arbitrarily mixed contributions of specular reflection, from the front surface, and diffusive reflection, from radiation that has penetrated into the sample. In those cases, an opposite direction peak can be observed, such as in Fig. 9b at 1690 cm^{-1}. A Kramers-Kronig transformation, which mathematically eliminates spectral distortion resulting from specular reflectance may sometimes be applied to improve reflectance spectra. However, this proved unsuccessful with our results, possibly due to the low signal and high noise, which resulted in alterations to the spectra that cannot be securely attributed to specular reflection.

3.2.1. Pristine experimental tars

The micro-FTIR analysis of pristine experimental pine tar (NDP01, Fig. 9a) resulted in a spectra that is difficult to match with previous literature, or to identify the majority of peaks indicating pine origin (Font et al., 2007; Martín-Ramos et al., 2018). Compared to pine tar, the micro-FTIR analysis of pristine experimental birch tar (NDP02, Fig. 9b) reveals clearer peaks associated with vibrational modes and functional groups of birch bark native markers, such as at approximately 1735, 920, and 888 cm^{-1} which may be attributed to betulin ν (C = O), lupeol ω (H-C-H) and betulinic acid ω (H-C-H), respectively (Cîntă-Pînzaru et al., 2012). However, there are numerous peaks and their respective vibrational modes occurring in similar wavenumbers for both different types of tars.

3.2.2. Weathered experimental

The quality of the micro-FTIR reflectance spectra deteriorates further for the weathered experimental tars. For pine tar (Hor3189, Fig. 10a), peaks at approximately 1725 cm^{-1} (ν C = O), 1465, 1383 cm^{-1} (δ CH_2 and CH_3), may be assigned to molecular vibrational modes related to pine origin, with the former at 1725 being unique to heated resin or tar (Font et al., 2007; Martín-Ramos et al., 2018). The spectra of weathered experimental birch tar (Hor3201, Fig. 10b) revealed only one peak that is exclusively assigned to a vibrational mode of birch bark (Cîntă-Pînzaru et al., 2012; Vahur et al., 2016), while multiple peaks are assigned to vibrational modes occurring in similar wavenumbers for the two different types of tars. As a result, the micro-FTIR spectra do not allow the identification of the material's birch bark origin.

3.2.3. Archaeological tar

As far as the archaeological samples are concerned, all points examined with micro-FTIR (Fig. 11a-d) provided multiple peaks that can be associated with organic materials. This allowed us to safely conclude that their residues were of organic nature. For each of these bone points, multiple peaks can also be associated with both pine tar and/or birch tar from the existing literature, and our experimental samples (Cîntă-Pînzaru et al., 2012; Font et al., 2007; Martín-Ramos et al., 2018; Vahur et al., 2016). These include peaks at around 1735, 1700–1710, 1595–1600, 1385–1390, and 890 cm^{-1}. NSM10 resulted in the clearest match with birch bark tar, however, almost all of the identifiable peaks, with the exception of 1734 cm^{-1}, can also be found in pine tar. For NSM16, NSM18 and NSM28, results are highly variable and of insufficient quality to securely identify peaks only associated with either pine or birch tar. As a result, micro-FTIR is unable to identify the residue as unambiguously either pine or birch tar.

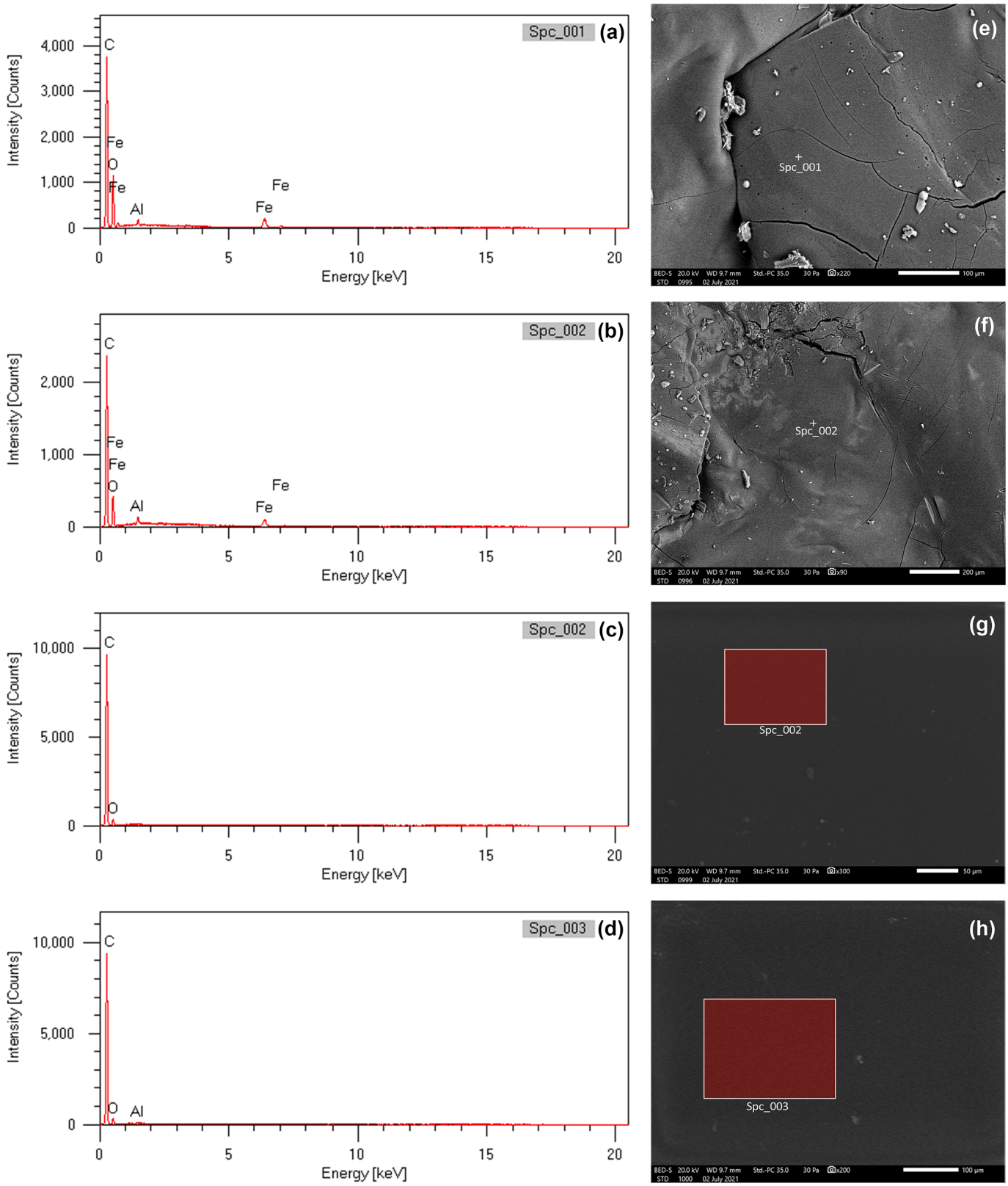

Fig. 3. (a), (b) EDS spectra collected from two locations on pristine experimental pine tar (NDP01). (c), (d) EDS spectra collected from two locations on pristine experimental birch tar (NDP02). (e)-(h) The corresponding backscattered SEM images. The two surfaces of birch bark tar in (g)) and (h) appear to be completely homogenous and showing no distinguishing features in the image. The crosses and coloured areas represent the locations that the EDS signal was recorded from.

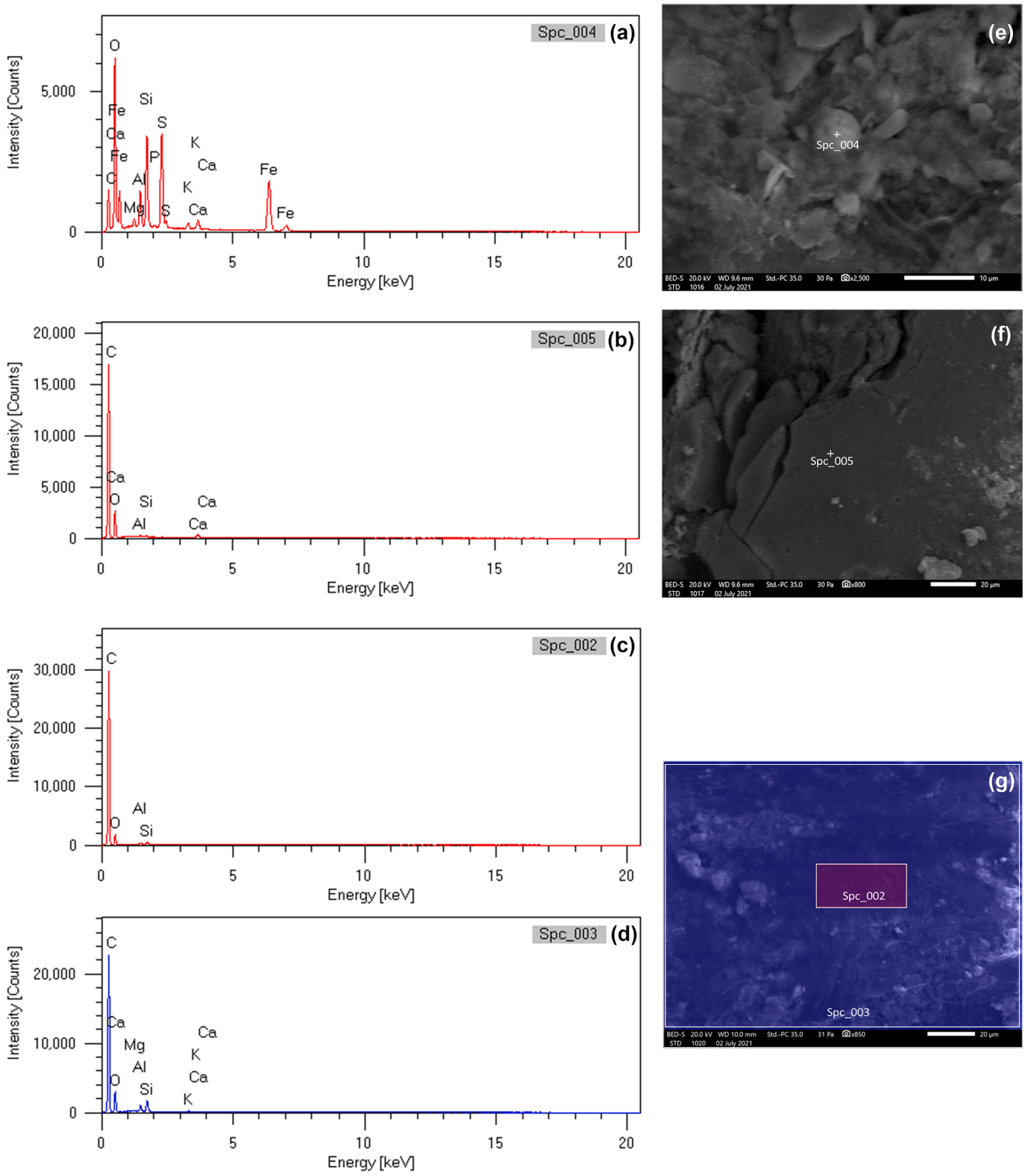

Fig. 4. (a), (b) EDS spectra collected from two locations on weathered experimental pine tar (Hor3189). (c), (d) EDS spectra collected from two locations on weathered experimental birch tar (Hor3201). (e)-(g) The corresponding backscattered SEM images. The crosses and coloured areas represent locations that the EDS signal was recorded from, in (g), Spc_003 was the entire image area.

3.3. XRD

3.3.1. Pristine experimental tars

The XRD analysis of the pristine experimental samples (Fig. 12) is quite straightforward. For both pristine pine tar (NDP01) and birch tar (NDP02), it was possible to recognise blunt curves on the XRD patterns. These features are located around 21° for pine tar (Fig. 12a), around 16° and 41.5° for birch tar (Fig. 12b) and are associated with a dominant amorphous part. This is a strong indication for the organic nature of the samples. Apart from the amorphous contribution, the XRD patterns of

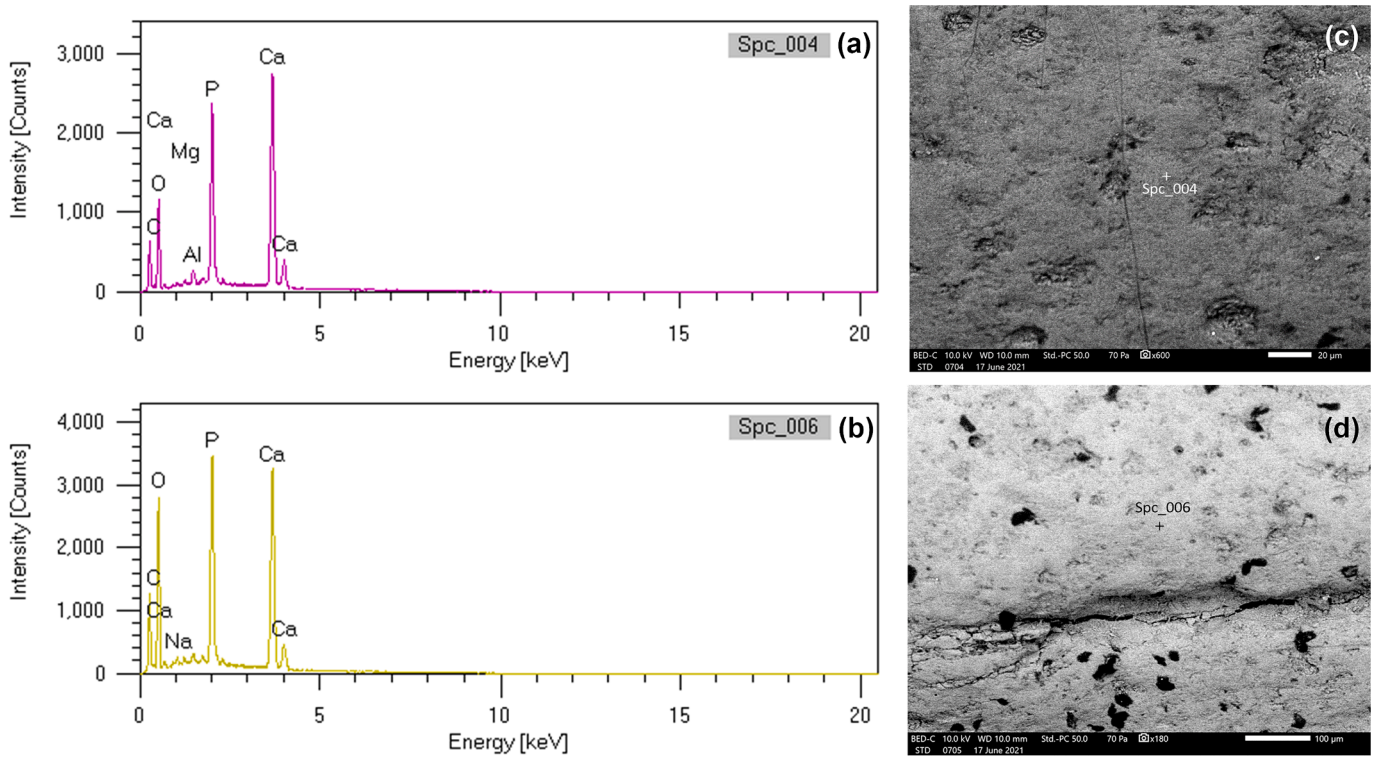

Fig. 5. (a)-(b) EDS spectra collected from two discolouration locations on NSM03. Spc_004 and Spc_006. (c)-(d) The corresponding backscattered SEM images. The crosses represent the locations that the EDS signal was recorded from.

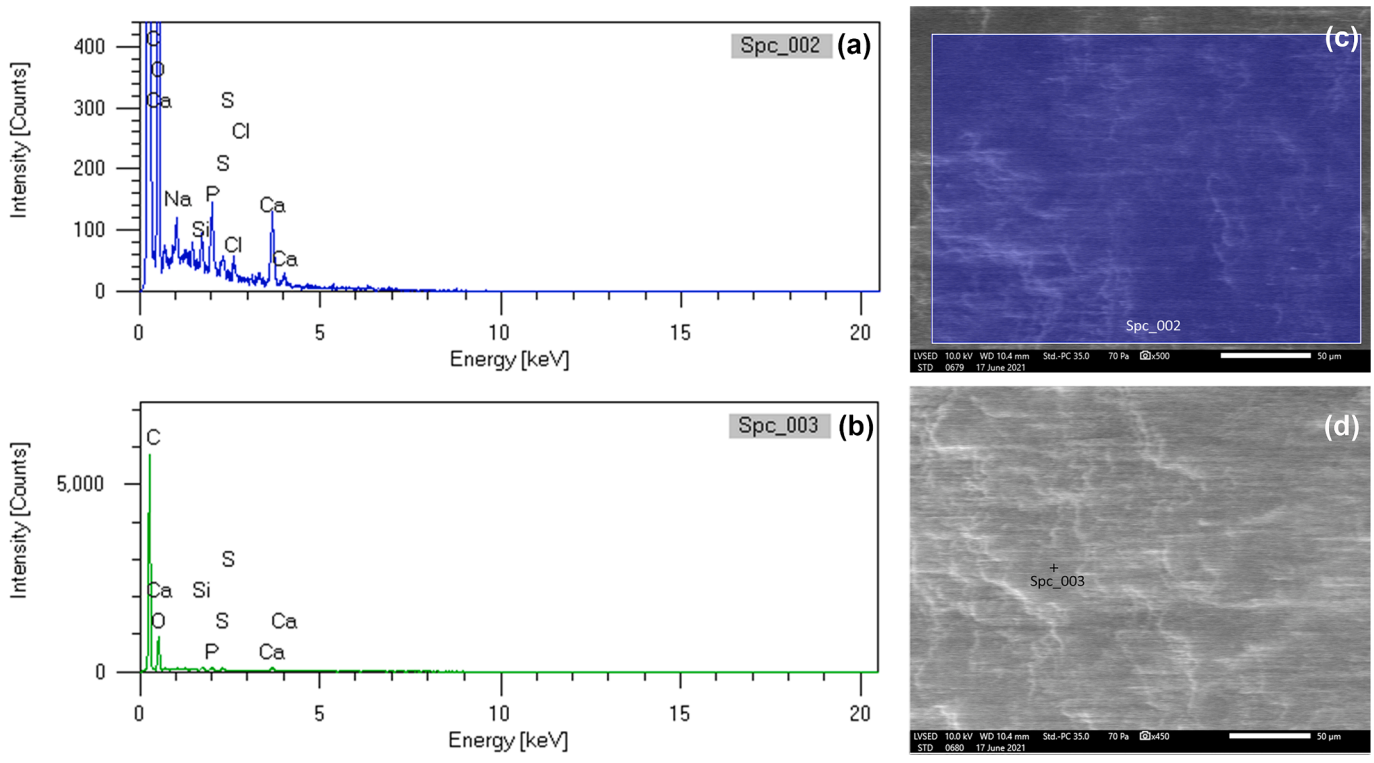

Fig. 6. (a)-(b) EDS spectra collected from two residue locations on NSM10. Spc_002 and Spc_003, (c)-(d) The corresponding backscattered SEM images. The crosses and coloured areas represent the locations that the EDS signal was recorded from.

the pristine experimental tars only show contribution from the underlying aluminium foil. The contribution is strong, even though the pristine experimental samples are deposited in thick layers, particularly birch tar. The patterns do not display any other features that could assist in differentiating between pine tar and birch tar.

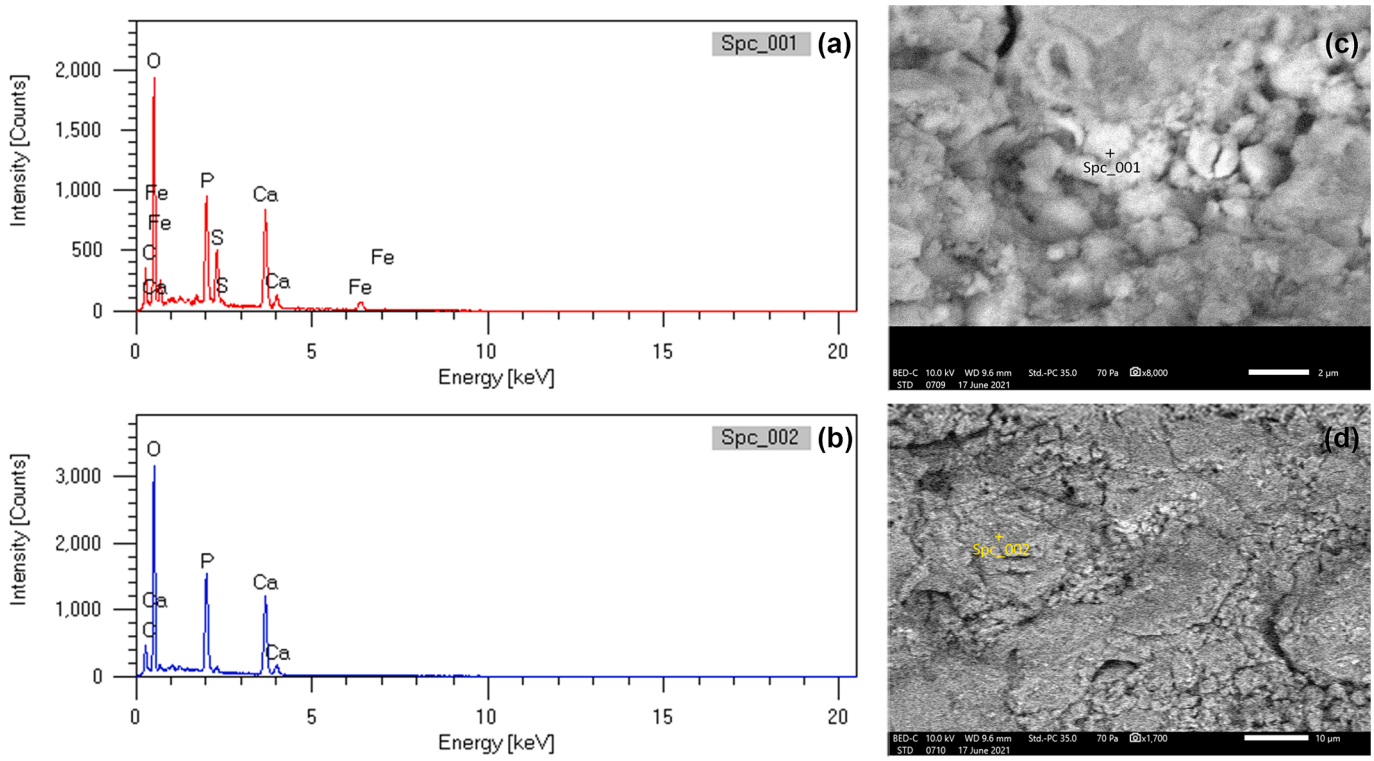

Fig. 7. (a)-(c) EDS spectra collected from two discolouration locations on NSM15. Spc_001 and Spc_002 (discolouration), (d)-(f) The corresponding backscattered SEM images. The crosses represent the locations that the EDS signal was recorded from.

3.3.2. *Weathered experimental tars*

No amorphous contribution is recognisable in the XRD patterns of either weathered experimental pine tar (Hor3189) or birch tar (Hor3201) (Fig. 13 and Fig. 14, respectively). The lack of amorphous contribution from the residue layer here can be due to the detrimental effect of natural degradation and by the residue layer being too thin. Quartz (SiO_2) and calcite ($CaCO_3$) are detected in both weathered experimental samples, identified in both locations on their residues that were analysed with XRD. These minerals are rather common components in archaeological sediments (Weiner, 2010). However, the detection of quartz can result from contribution of the flint. When analysing adhesive residues from unknown archaeological artefacts, we cannot dismiss the possibility of quartz being included as an additive to the adhesive mixture (Charrié-Duhaut et al., 2013). XRD does not allow us to understand whether the contribution results from the substrate, an adhesive additive, or the sediment. This distinction is very important when analysing archaeological material. Combining the method with light microscopy on the analysis location, would be able to provide some indications on the matter based on the observed surface morphology. The XRD analysis on one of the analysed locations of the weathered pine tar residue (Fig. 13a) reveals another crystalline phase of silicon oxide (SiO_2), cristobalite. The reference bars for cristobalite are displayed in green. On the same analysis location (Fig. 13a), calcite is also detected, indicted on the pattern with blue reference bars.

Weathering, even for a three-year period, was decisive for the detection of amorphous-related features in the diffractogram. XRD is thus unable to verify the organic nature of both weathered experimental tars. As a result, it is expected that it will be hard or even impossible to detect the amorphous contribution in archaeological samples as well. Similar to the pristine experimental samples, the patterns do not show any other features useful for distinguishing between pine tar and birch tar.

3.3.3. *Archaeological tar*

Based on the XRD analysis of the archaeological artefacts (Figs. 15, 16, 17, 18, 19), it is surprising that an amorphous part was detected in the pattern of the analysis location 1 of NSM10 residue (Fig. 15a). The amorphous contribution is revealed in the form of a large blunt curve centred around 18° 2 θ in the pattern of the black residue on the bone point's surface. There was no such feature observed in the diffractogram of the remaining analysis locations of the same bone point or in any of the other bone points. This implies the organic nature of the black residue on NSM10.

The discoloured and residue locations, show a very strong contribution of hydroxyapatite. The detection of this inorganic bone component in the XRD patterns was anticipated, based on the strong contribution of the substrate material, aluminium and flint, already observed in the diffractograms collected from the experimental samples. We should underline that hydroxyapatite signal is detectable in almost every single one of the XRD readings. This holds when the discolouration is only a thin film of black staining, like in the case of NSM03 (Figure S7), but it is also the case for three-dimensional residues that are a few millimetres thick. For instance, hydroxyapatite is detectable in the pattern of the NSM10 residue (Fig. 15a). It is not detectable in any of the two readings collected from the residue on NSM18 (Fig. 17a and b). This can imply that the NSM18 residue is thicker and does not allow for the contribution of the bone substrate to reach the XRD detector. Two slightly different crystalline structures of hydroxyapatite are detected among the bone points' XRD patterns, $Ca_5(PO_4)_3(OH)$ and the less conventional $Ca_{4.86}(H_{0.222}(PO_4)_3)(OH)_{0.942}$. This small variation of the stoichiometric ratio is probably related to defects in the hydroxyapatite crystal. The difference in their diffraction patterns is negligible for the purpose of this study.

Quartz (SiO_2) and calcite ($CaCO_3$) have a strong presence in the residue diffractograms too. They can both be associated with the post-depositional material resulting from burial, since, as already discussed, these minerals are very common in archaeological sediments (Weiner, 2010). Quartz might also be an additive to the organic residue, but as already mentioned, XRD cannot offer further insight on distinguishing its origin. An additional phase, calcium silicate ($CaSiO_3$),

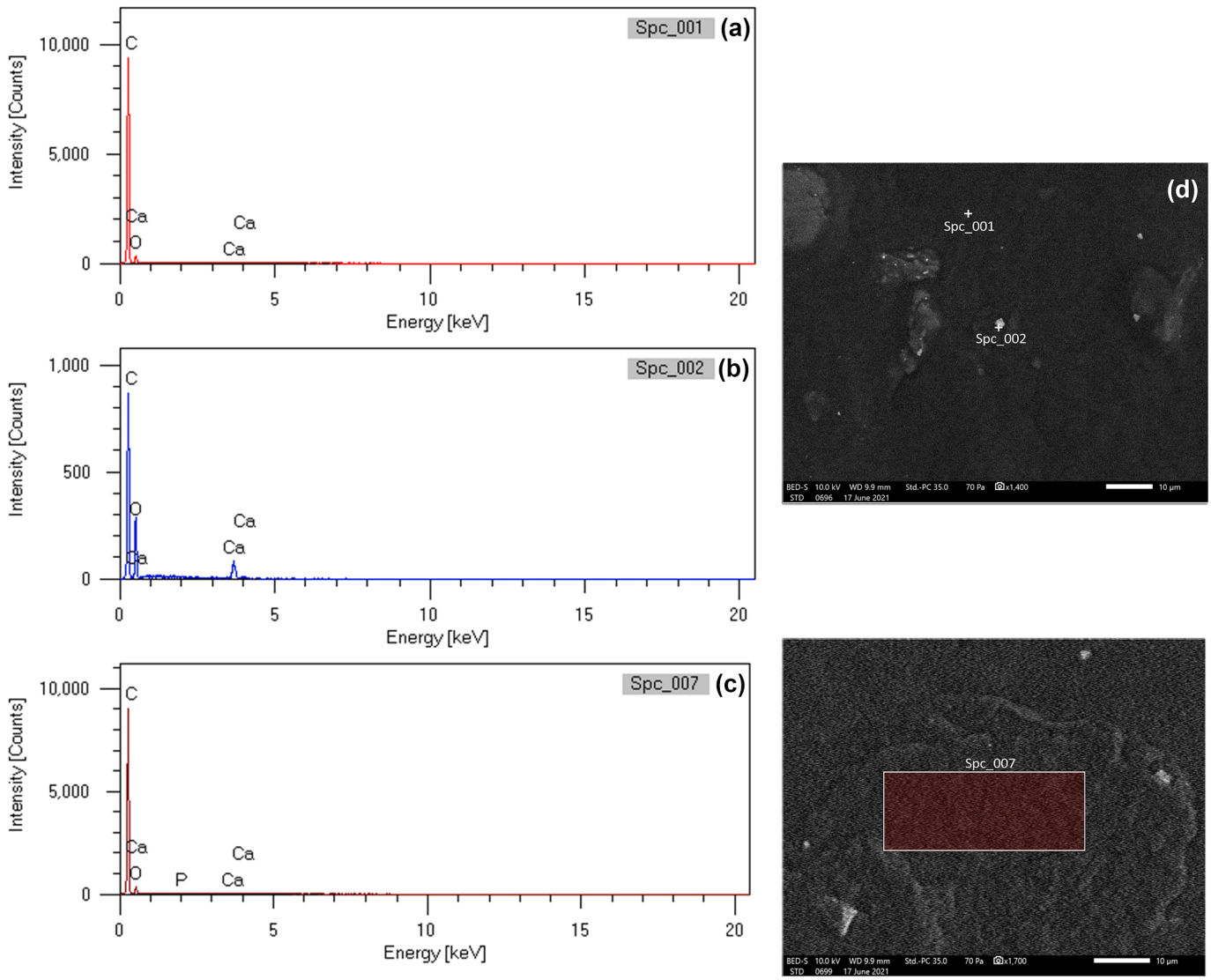

Fig. 8. (a)-(c) EDS spectra collected from three locations on the NSM16 residue. (d), (e) The corresponding backscattered SEM images. The crosses and coloured areas represent the locations that the EDS signal was recorded from.

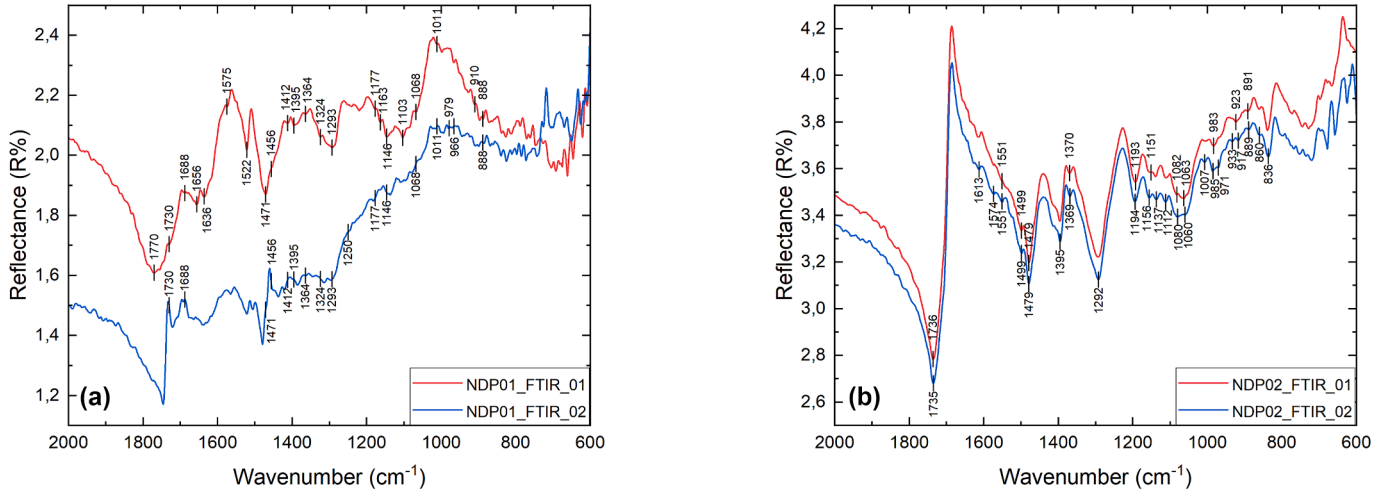

Fig. 9. (a) Micro-FTIR spectra collected from two locations (01 and 02) on pristine experimental pine tar (NDP01). (b) Micro-FTIR spectra collected from two locations (01 and 02) on pristine experimental birch tar (NDP02). Details of micro-FTIR spectra in the region of 2000–600 cm^{-1}.

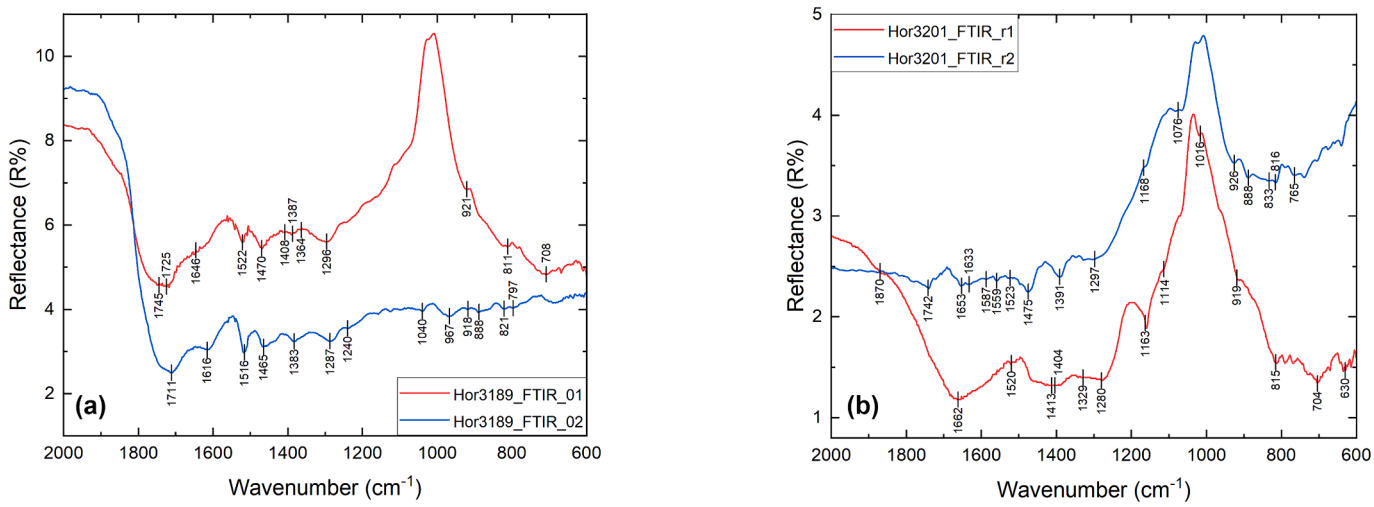

Fig. 10. (a) Micro-FTIR spectra collected from two locations (r1 and r2) on the weathered experimental pine tar (Hor3189) hafting adhesive. (b) Micro-FTIR spectra collected from two locations (r1 and r2) on the weathered experimental birch tar (Hor3201) hafting adhesive.

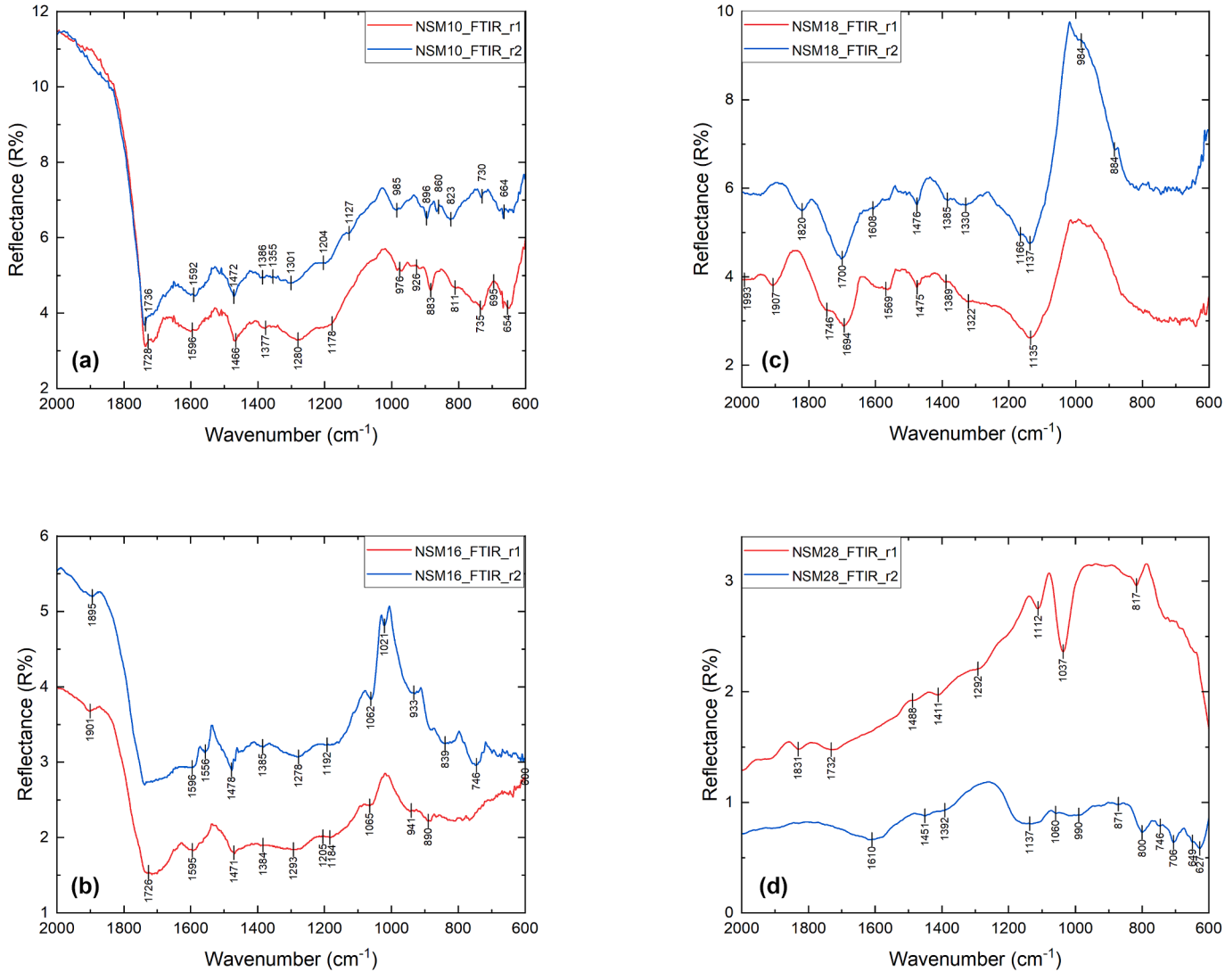

Fig. 11. Micro-FTIR spectra collected from two locations on the residue (r1 and r2) of (a) NSM10, (b) NSM16, (c) NSM18 and (d) NSM28. Note that no peaks are associated with pine tar or birch tar for NSM16. Only one band is assigned to pine tar for NSM28.

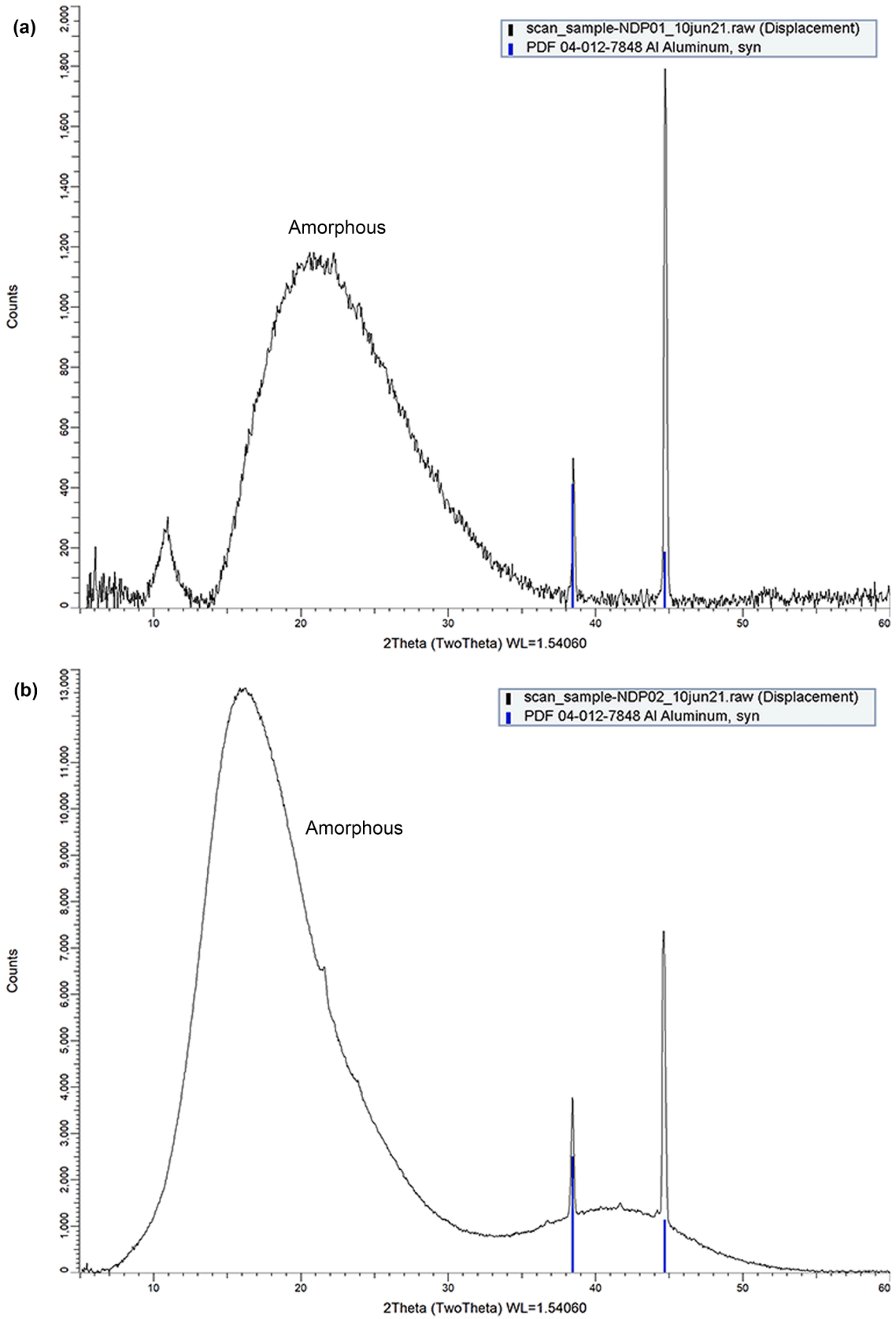

Fig. 12. XRD pattern collected from (a) pristine experimental pine tar (NDP01) and (b) pristine experimental birch tar (NDP02). The blue bars indicate the peak positions and intensities of aluminium (Al), using the ICDD pdf4 database. The pattern demonstrates amorphous matter and Al contribution. (For interpretation of the references to colour in this figure legend, the reader is referred to the web version of this article.)

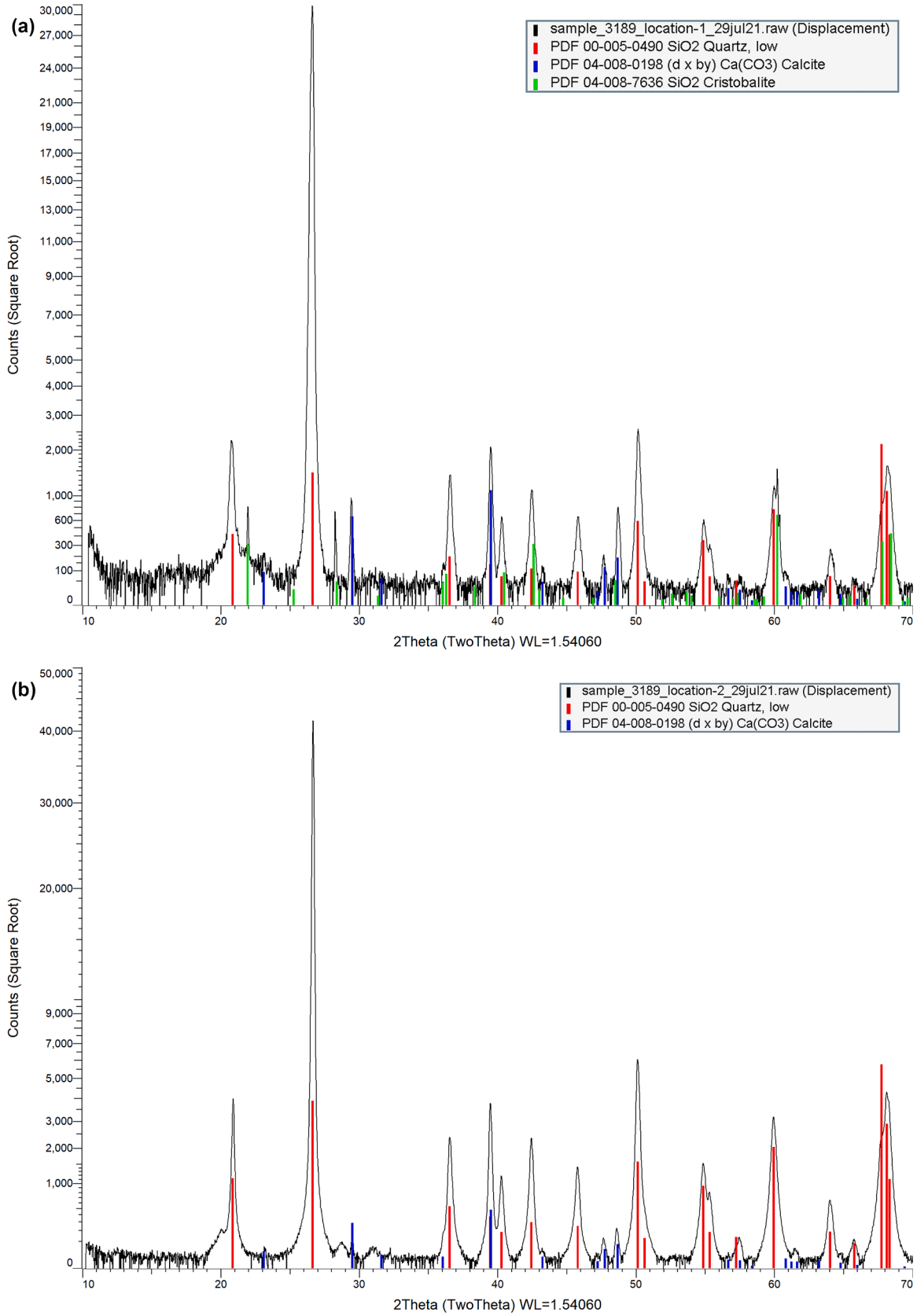

Fig. 13. XRD patterns collected from two locations on weathered experimental pine tar (Hor3189). (a) location 1, (b) location 2. The coloured bars indicate the reference peak positions and intensities of possibly present crystalline phases, using the ICDD pdf4 database. quartz (SiO_2) in red, calcite ($CaCO_3$) in blue and cristobalite (SiO_2) in green. Square root scaling is used for the intensity. (For interpretation of the references to colour in this figure legend, the reader is referred to the web version of this article.)

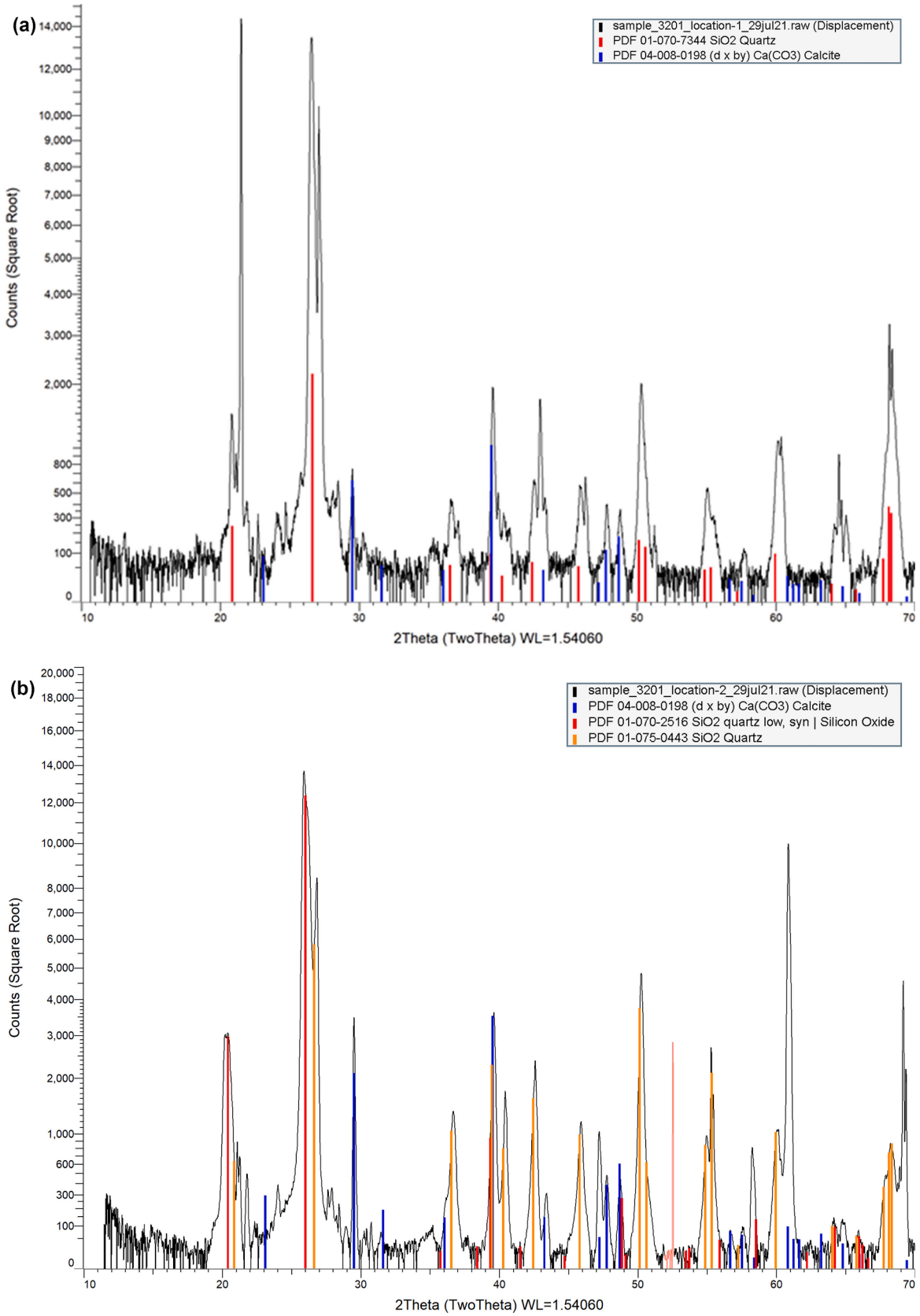

Fig. 14. XRD patterns collected from two locations on weathered experimental birch tar (Hor3201). (a) location 1, with calcite reference XRD pattern superimposed, (b) location 2. The coloured bars indicate the reference peak positions and intensities of possibly present crystalline phases, using the ICDD pdf4 database. calcite ($CaCO_3$) in blue and two quartz (SiO_2) structures in red and orange. Square root scaling is used for the intensity. (For interpretation of the references to colour in this figure legend, the reader is referred to the web version of this article.)

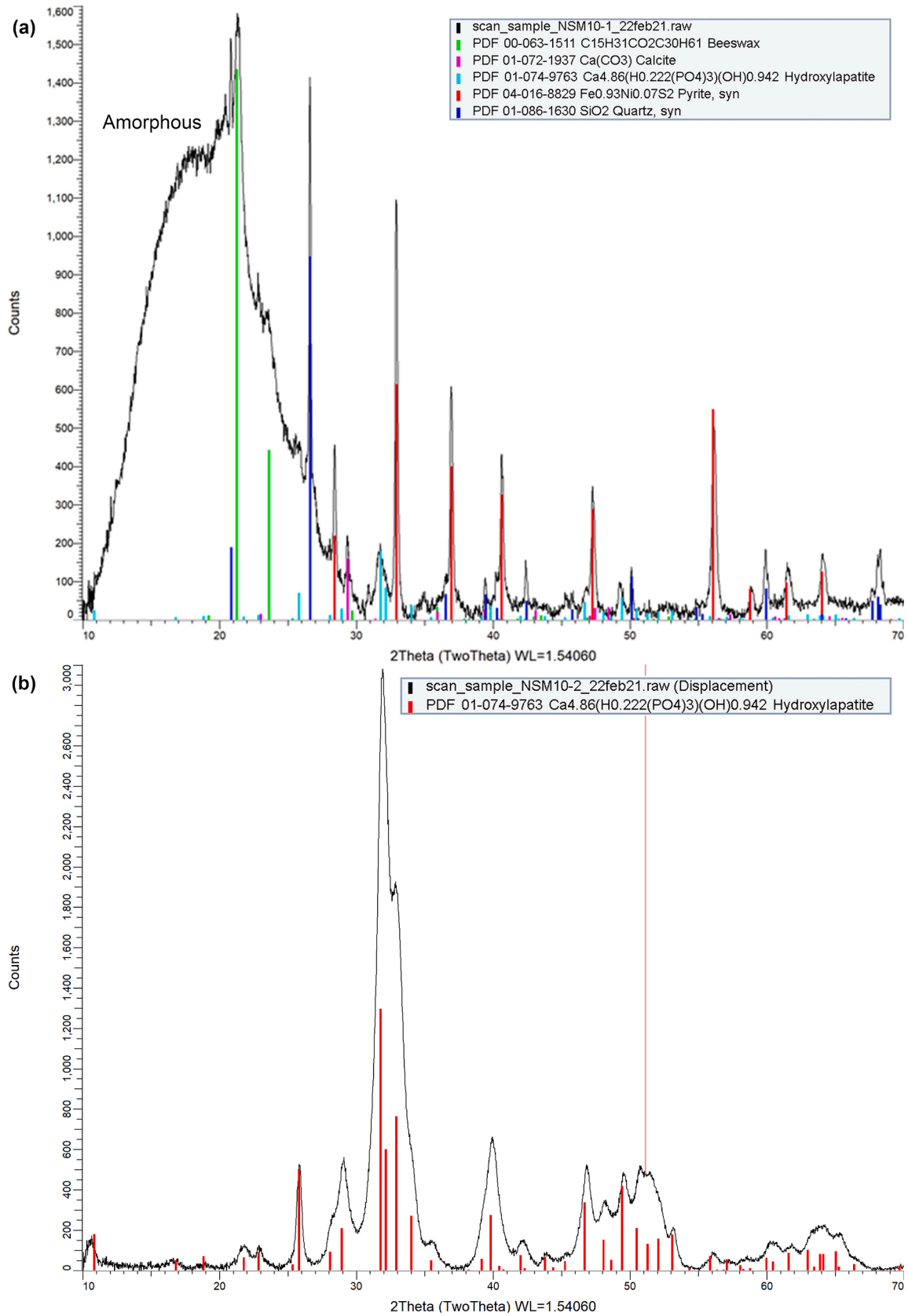

Fig. 15. XRD patterns collected from two locations on NSM10. (a) location 1 (residue), (b) location 2 (discolouration near the point's edge). The coloured bars provide the reference peak positions and intensities of the possibly present crystalline phases, using the ICDD pdf4 database. (a) beeswax ($C_{15}H_{31}CO_2C_{30}H_{61}$) in green, calcite ($CaCO_3$) in magenta, hydroxyapatite($Ca_{4.86}(H_{0.222}(PO_4)_3)(OH)_{0.942}$) in turquoise, pyrite ($Fe_{0.93}Ni_{0.07}S_2$) in red and quartz ($SiO_2$) in blue, (b) hydroxyapatite ($Ca_{4.86}(H_{0.222}(PO_4)_3)(OH)_{0.942}$) in red. (For interpretation of the references to colour in this figure legend, the reader is referred to the web version of this article.)

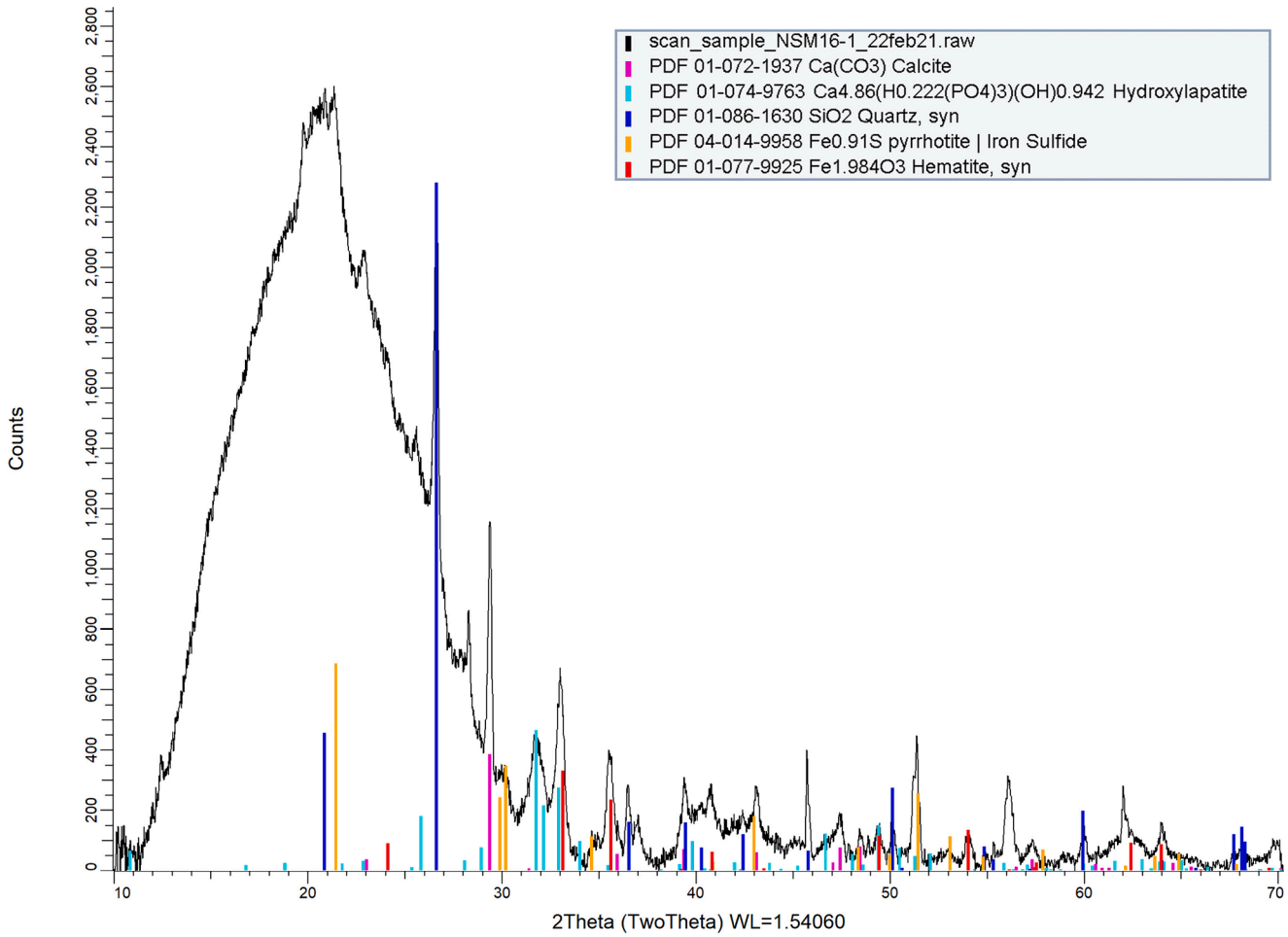

Fig. 16. XRD patterns collected from location 1 black residue) on NSM16. The coloured bars provide the peak positions and intensities of the possibly present crystalline phases, using the ICDD pdf4 database. calcite ($CaCO_3$) in magenta, hydroxyapatite ($Ca_{4.86}(H_{0.222}(PO_4)_3)(OH)_{0.942}$) in turquoise, quartz ($SiO_2$) in blue, pyrrhotite ($Fe_{0.91}S$) in orange and hematite ($Fe_{1.984}O_3$) in red. (For interpretation of the references to colour in this figure legend, the reader is referred to the web version of this article.)

was detected on the pattern collected from the residue of NSM28, probably because of sediment contribution.

Different crystalline forms of iron sulphides are also detected with XRD. Pyrite, in different crystalline forms with varying stoichiometric ratios, from the conventional FeS_2 lattice to $FeS_{1.92}$ and $Fe_{0.93}Ni_{0.07}S_2$, are detected in the XRD patterns of the residues on NSM10 (Fig. 15a) and NSM18 (Fig. 17a-b, Fig. 18). Iron sulphides such as pyrite can result from the degradation of organic matter in anoxic marine environments by sulphate-reducing bacteria (Schippers and Jorgensen, 2002). Seeing that this collection of bone points has been exposed to marine environment for a long period of time, the detection of pyrite with XRD acts as an indication for the presence of some organic matter in the surface of the point in question.

Finally, some possible additive materials are falsely detected in the XRD patterns. Beeswax ($C_{15}H_{31}CO_2C_{30}H_{61}$) is one of the phases possibly identified in the pattern of the residue on NSM10 (Fig. 15a). This could suggest that the residue on NSM10 is a mixture of birch tar, as confirmed by GC-MS, and beeswax, as detected by XRD. However, beeswax was not detected in the GC-MS and micro-FTIR results of NSM10 (Aleo et al., manuscript in preparation). Also, a closer look on the pattern of Fig. 15a reveals that only two peaks match with the beeswax reference. Due to the lack of beeswax detection in GC-MS and in our vibrational spectra, the detection of beeswax here by XRD is probably a result of misinterpretation. Another important observation is the detection of hematite in the XRD patterns of the NSM16 residue. It is likely that hematite was used in this case as an additive to the adhesive mixture, probably as part of an ochre mineral (Kozowyk et al., 2016; Wadley, Williamson, & Lombard, 2004).

The results collected from the XRD analysis of the archaeological samples are summarised in Table 4.

4. Discussion

Our study shows that SEM coupled with EDS analysis is a useful tool of analysis for the purpose of this study. In all three stages of organic material degradation (pristine experimental, weathered experimental, aged archaeological) the generated spectra are clear, and their carbon peak intensity is not significantly affected by degradation. This enables the analyst to confidently draw a conclusion on the organic content of the material under examination. In our case, demonstrating that the residues lying on the surface of the bone points are organic, paves the way for the macro-wear and micro-wear analysis to prove them as hafting remnants (Aleo et al., 2023). It must be stressed that there were no features detected in the EDS spectra of the experimental or archaeological samples that could be indicative of the origin of the tars under examination, i.e. pine versus birch. The information provided by SEM-EDS is limited mainly to the verification of a residue being organic. Elements related to the environment of weathering can also be detected, possibly providing some insight into its provenance, like in the case of iron and sulphur. In a general case of analysing unknown archaeological samples, the EDS elemental analysis would also be able to provide indications on possible additives to the adhesive mixture.

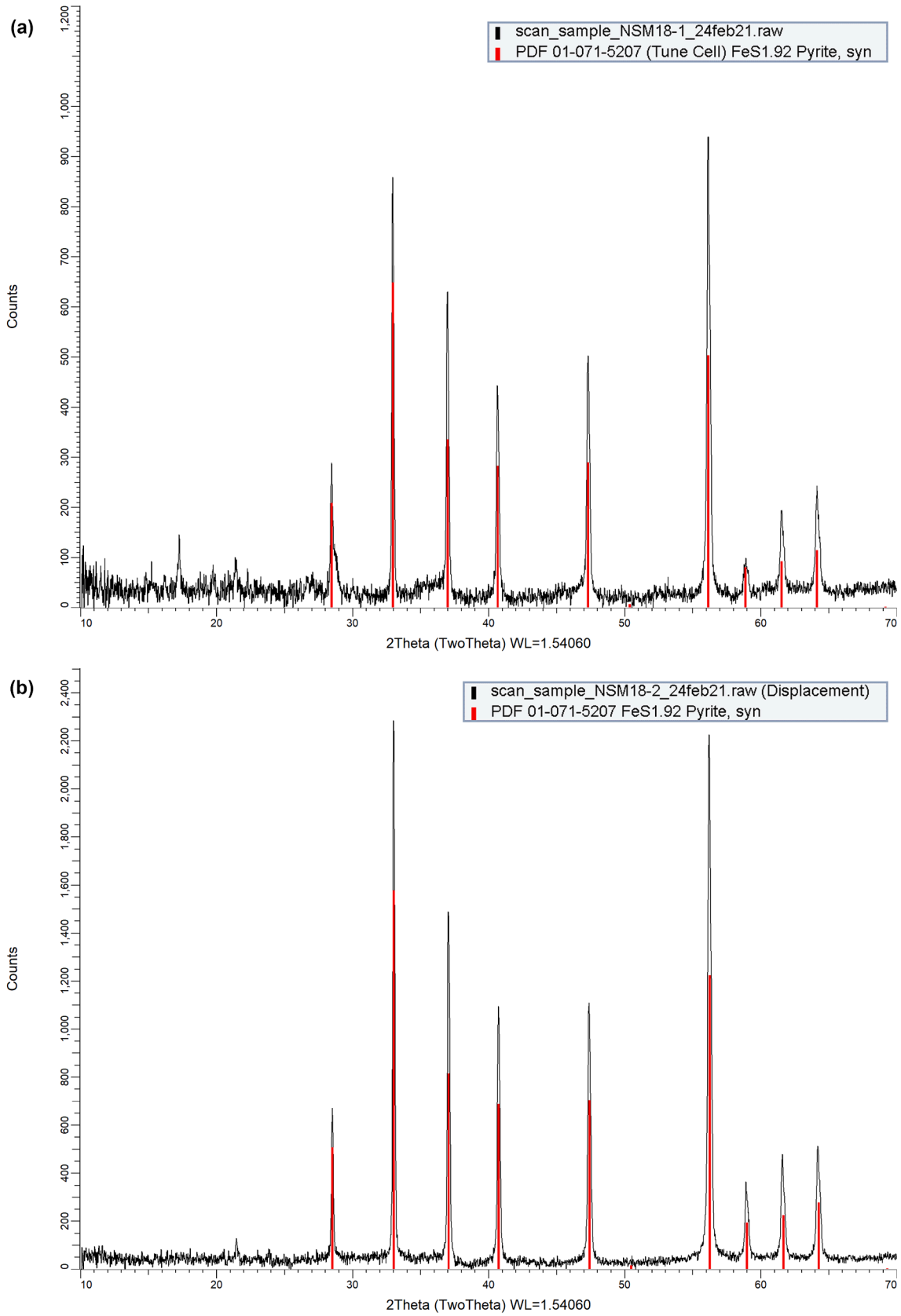

Fig. 17. XRD patterns collected from two locations on NSM18. (a) location 1 (black residue), (b) location 2 (red/brown residue). The red bars provide the reference peak positions and intensities of the possibly present crystalline phase, using the ICDD pdf4 database. pyrite ($FeS_{1.92}$). (For interpretation of the references to colour in this figure legend, the reader is referred to the web version of this article.)

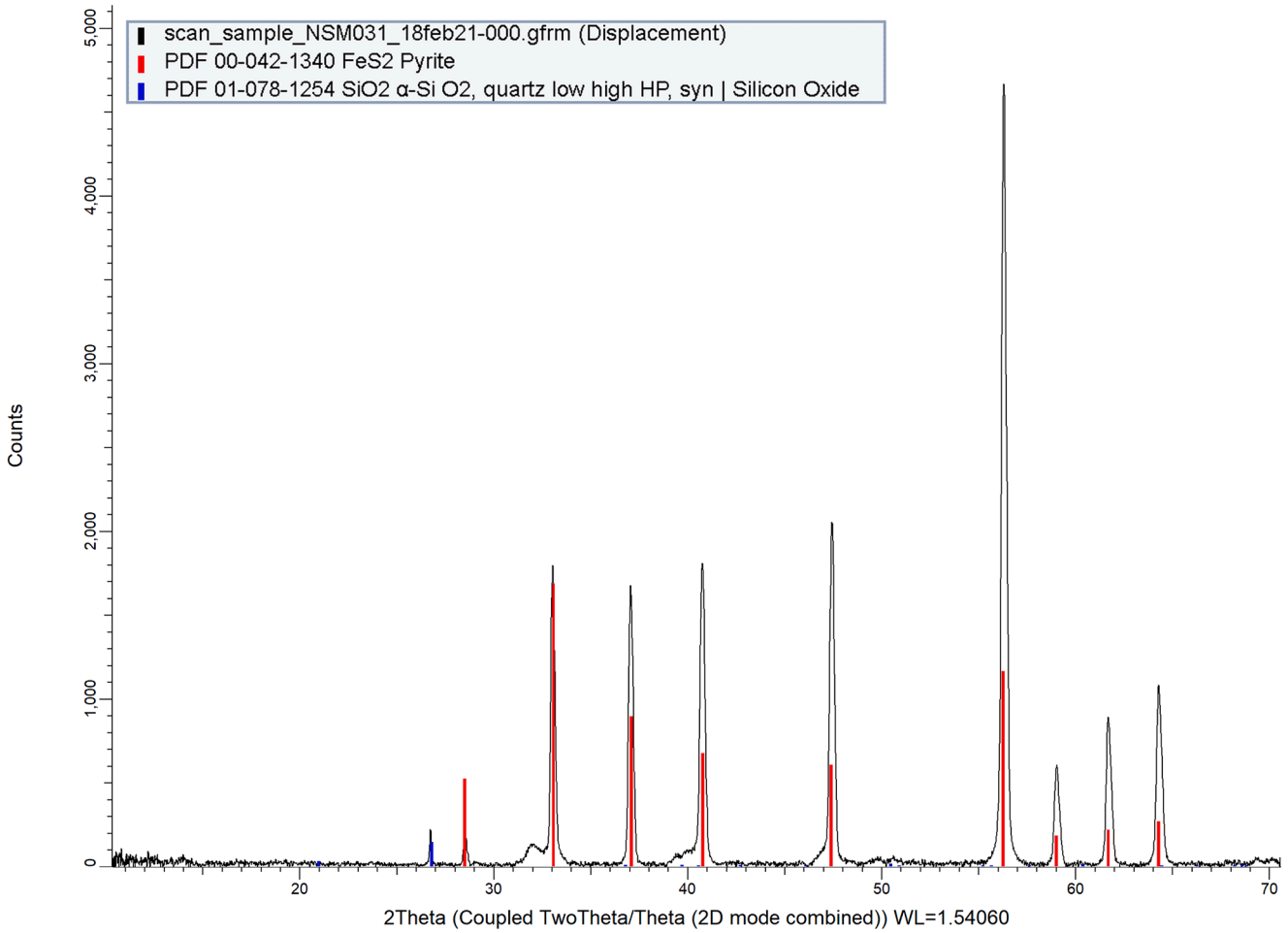

Fig. 18. XRD pattern collected from the inner surface of NSM31 (loose residue collected from NSM18). The coloured bars provide the reference peak positions and intensities of the possibly present crystalline phases, using the ICDD pdf4 database. pyrite (FeS_2) in red and (c) quartz (α-SiO_2). (For interpretation of the references to colour in this figure legend, the reader is referred to the web version of this article.)

Our EDS results, collected from experimental and archaeological samples, do not corroborate with Dinnis et al. (2009), Pawlik (2004) and Pawlik & Thissen (2011), who associate the presence of calcium, potassium and/or sulphur in the EDS spectra of experimental or archaeological samples with birch tar. In our work, calcium, potassium and sulphur are only present in the spectra of weathered experimental materials, not of the pristine samples. Furthermore, calcium is present in the spectra of the NSM10 and NSM18 archaeological residues, which have been identified by GC-MS as birch tar. This results either from the bone's hydroxyapatite, or, most probably, from sediment deposition. On the other hand, potassium is not detected in any locations of the bone points, neither on the residues, nor on the bare bone. The presence of sulphur here is interpreted as the result of decomposition in the marine environment. Calcium, potassium and/or sulphur are related to weathering of the organic materials and linking these elements with birch tar production is not accurate.

Our knowledge can be further complimented by the XRD analysis. The results of the pristine experimental samples and one of the archaeological bone points (NSM10) implied an organic content by broad blunt curves in the diffraction patterns. Furthermore, the presence of pyrite, resulting from the marine environment related to our archaeological samples, reinforced the indications concerning their organic nature. It thus seems that XRD can simultaneously offer some insight on the provenance of unknown archaeological artefacts, by exposing phases that are characteristic to their environments. Lastly, XRD can also serve for the identification of inorganic crystalline additives, like ochre, as well as the detection of post-depositional sediment particles overlaying the adhesive surface. Therefore, our analysis shows that, while there is no evidence that can help us in identifying or distinguishing the tars in any of the degradation states, XRD is a useful, but complimentary tool.

Identifying the tars through micro-FTIR proves very challenging, particularly for weathered and significantly aged samples. Yet, it is the best out of our selected methods. In addition, our analysis demonstrates that this spectroscopic technique is also able to verify the organic nature of adhesives, no matter their state of degradation, with results that corroborate with those of SEM-EDS.

The main complication with distinguishing between pine tar and birch tar using reflectance infrared spectra is issued by many vibrational modes being close or common between markers of pine and birch tar, the general high signal to noise ratio of the spectra, and the combination of specular and diffuse reflectance. The distinction between the two types of tars for aged experimental samples and archaeological materials is further complicated due to the severe effect of natural decay. Based on the literature, a small number of the peaks detected for NSM10, NSM16, NSM18 and NSM28 can be exclusively assigned to pine or birch tar. Most detected peaks are assigned to vibrations that occur for both tars, with the exception of 1734 cm^{-1} in NSM10, which provided the single best quality spectra for the archaeological material. It is thus impossible to reliably identify the residues on all of the archaeological bone points as a pine or birch product through FTIR analysis. Further, most IR spectra have very low reflectance, indicating that most of the IR light was

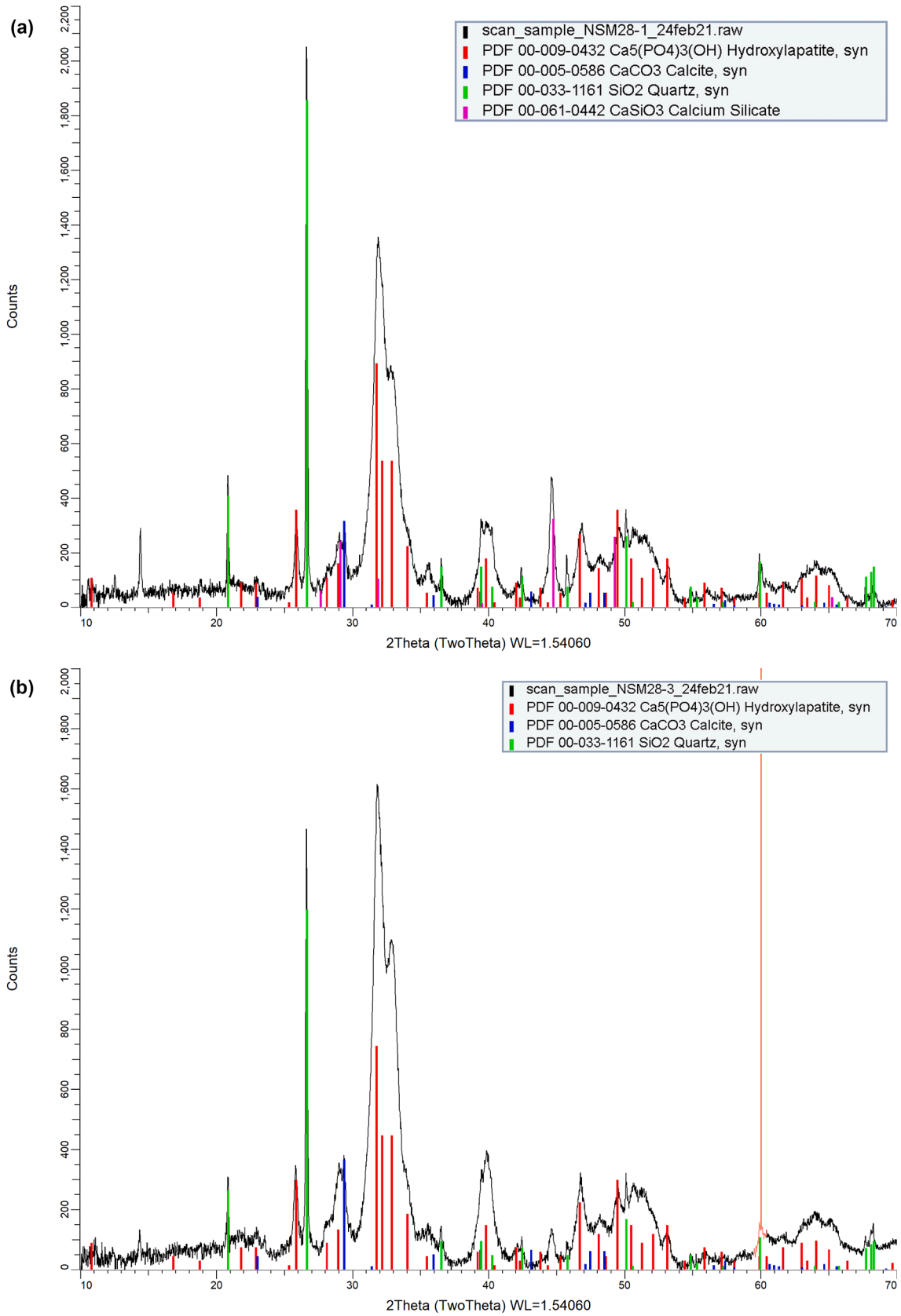

Fig. 19. XRD patterns collected from two locations on NSM28. (a) location 1 (discolouration near the point's edge), (b) location 3 (discolouration near the point's barbs). The coloured bars provide the reference peak positions and intensities of the possibly present crystalline phases, using the ICDD pdf4 database. hydroxyapatite ($Ca_5(PO_4)_3(OH)$) in red, calcite ($CaCO_3$) in blue, quartz (SiO_2) in green and calcium silicate ($CaSiO_3$) in magenta. (For interpretation of the references to colour in this figure legend, the reader is referred to the web version of this article.)

Table 4
Summary of XRD results for the residue/discolouration analysis locations of archaeological bone points.

Sample	Location	Description	Crystal phase						
			Amorphous	Pyrite / Pyrrhotite	Beeswax	Quartz	Calcite	Calcium silicate	Hematite
NSM010	1	black residue	√	√	√	√	√	√	x
	2	black residue at tip	x						
NSM16	1	black residue	x	√	x	√	√	x	√
NSM018	1	black residue	x	√	x	x	x	x	x
	2	red/brown residue	x	√	x	x	x	x	x
	NSM31	loose residue, inner surface	x	√	x	√	x	x	x
NSM028	1	black residue	x	x	x	√	√	√	
	3	black residue at tip	x	x	x	√	√	x	

absorbed, resulting in weaker/noisier reflectance spectra. The analyses should thus be performed with great care, since the sample's surface characteristics can result in measuring low reflections.

The identification of pine tar is further complicated due to its chemical affinity to pine resin. The two pine products share their native biomarkers. In addition, the markers of aged pine resin coincide with some of the degradation markers of pine tar. It is thus difficult to deduce whether the presence of degradation markers is the result of natural decay of pine resin or are caused by anthropogenic heat input to produce tar. The markers that can guarantee pine tar are retene, methyl dehydroabietate and 1,7-dimethylphenanthrene (Rageot et al., 2016).

Invasive ATR-FTIR has been applied to identify archaeological pine pitch (e.g. Odegaard et al., 2014), resulting from heat processing of pine resin in the absence of wood. Destructive transmission FTIR has been applied to compare the spectral features of colophony, pine pitch (pine resin heated in the absence of wood) and tar (Font et al., 2007) as references for the identification of archaeological amphorae coatings. Font et al. (2007) produce very clear FTIR transmission spectra of their archaeological samples that match their pristine reference experimental samples well, thus enabling identification. They indicate the emergence of a few bands related to hydroxyls, ketones and aromatic groups that are distinctive for pine wood tar, versus colophony.

It must be noted that the available literature is based on invasive, even destructive applications of FTIR that require sampling. This methodology does not fulfil the requirements for non-destructive *in situ* analysis, which is essential for the archaeological research of many artefacts. *In situ* spectra collection of weathered experimental and archaeological residues in reflectance, like in our work, results in spectra that are less clear and necessitate detailed assignment of the bands to vibrational modes of interest to enable identification. Such a detailed designation of the pine tar spectra bands and their assigned vibrational modes to specific native versus degradation markers is not included in the available literature. Without this information, it is unclear which bands are related to human-induced tar production processes. Therefore, it might be possible to identify the pine origin of an adhesive, but we cannot reliably conclude on its tarry nature by applying FTIR independently. As far as the identification of birch bark tar through band assignment is concerned, Cîntă-Pînzaru et al. (2012) include assignments of the ATR-FTIR bands for their birch bark samples to lupeol, betulin and betulinic acid. Technically, these native biomarkers are unable to distinguish birch tar from untreated birch bark. However, combined with the functional context and visual inspection of the archaeological residues, it is easy to conclude on tar of birch origin. The work by Cîntă-Pînzaru *et al.*, among others, has been used by Rao *et al.* (2009) to identify residues in Chinese prehistoric pottery as birch bark tar, through their transmission FTIR spectra. However, their bands are assigned to vibrations that are not exclusive to birch bark tar, as they are also associated with pine resin and/or pine tar (Font et al., 2007). They particularly state that the emergence of a band at 886 cm^{-1} indicates birch tar versus pine resin. However, Font et al. (2007) state that an 888 cm^{-1} band is characteristic of pine pitch/tar, with respect to pine resin. This contradiction illustrates the problematic and biased use of band assignments that are not exclusive to one tar for identification. It also highlights the need for further research on band assignment to particular degradation markers, characteristic of tar production. This research needs to take into account the complications issued by decay and the need for non-invasive analysis in the identification process. Our work, issuing the FTIR study of weathered experimental materials *in situ* and in non-destructive, non-invasive reflectance mode is thus important, as it is more representative of the archaeological record.

ATR FTIR can enhance infrared spectra obtained with better visualization of weak bands, as they are generally less subject to background effects and easier to interpret. ATR spectra of experimental samples can be utilised as additional references for spectra comparison, but this method does not fulfil the criteria for non-destructive and non-invasive characterisation of archaeological material. In rare circumstances, ATR FTIR may be applied directly on an artefact, however, this comes with a risk of damaging fragile materials. Other methods, such as Raman vibrational spectroscopy, could be better suited for the differentiation of tars. However, they should be thoroughly tested for their ability to identify weathered tars in an exclusively non-destructive manner. Incorporating more methods in such a systematic attempt is promising. However, distinguishing different archaeological tars is currently best done through destructive methods.

5. Conclusion

Aiming to differentiate archaeological pine wood tar and birch bark tar, three different non-destructive methods were tested in this study. SEM-EDS, FTIR microspectroscopy and XRD were used to analyse a set of experimental adhesive replicas, as well as a collection of Mesolithic bone points from Doggerland (Dutch North Sea).

Although the SEM-EDS analysis cannot contribute to the identification of tars, the EDS spectra are a very powerful and straightforward tool for organic verification and can also reveal information on the environment of burial for archaeological artefacts. Crystalline phases used as additives to the tar mixture, for example beeswax or ochre, or related to the environment of burial can be detected through XRD. While indications of amorphous organic contributions might be visible in the XRD patterns, identification of the amorphous constituents is not possible. Infrared spectroscopy emerged as the most valuable technique for non-destructive analysis, since it can independently verify archaeological tar material as organic and offer useful evidence towards tar identification and distinction. However, the complexity of identifying archaeological tars is clear: birch bark and pine wood tar markers often overlap and are not unique; it is difficult to distinguish resin and tar from the native markers for pine wood using reflectance FTIR. Further research is needed to enrich the FTIR libraries with weathered reflectance tar spectra, to explore techniques for enhancing the quality of the spectra, and to identify vibrational modes characteristic of degradation markers that guarantee for tar production processes.

CRediT authorship contribution statement

Myrto Despotopoulou: Conceptualization, Data curation, Formal analysis, Methodology, Visualization, Writing – original draft, Writing –

review & editing. **Geeske H.J. Langejans:** Conceptualization, Methodology, Resources, Supervision, Writing – review & editing. **Ruud W. A. Hendrikx:** Data curation, Formal analysis, Writing – review & editing. **Ineke Joosten:** Data curation, Formal analysis, Writing – review & editing. **Marlies Nijemeisland:** Resources, Writing – review & editing. **Johannes A. Poulis:** Resources, Writing – review & editing. **Paul R.B. Kozowyk:** Conceptualization, Methodology, Resources, Writing – review & editing.

Data availability

Data will be made available on request.

Acknowledgements

We would like to thank the Rijksmuseum van Oudheden in Leiden, the Netherlands and the amateur archaeologists/palaeontologists Cedric Heins, Henk Houtgraaf and Peter Soeters for providing generous access to their collections and allowing us to analyse the archaeological artefacts. We are also thankful to Prof. Annelou van Gijn and the Laboratory for Artefact Studies at Leiden University for providing logistical and analytical support for the experiments.

Appendix A. supplementary material

Supplementary data to this article can be found online at https://doi.org/10.1016/j.jasrep.2024.104571.

References

Adriaens, A., Dowsett, M.G., 2004. Electron microscopy and its role in cultural heritage studies. Comprehens. Anal. Chem. Elsevier 73–128.

Aleo, A., Kozowyk, P.R.B., van Gijn, A., Baron, L.I., Langejans, G.H.J., 2023. The dynamic lives of osseous points from Late Palaeolithic/Early Mesolithic Doggerland: A detailed functional study of barbed and unbarbed points from the Dutch North Sea. PLOS ONE 18(8): e0288629. https://doi. org/10.1371/journal.pone.0288629.

Amkreutz, L., Spithoven, M., 2019. Hunting beneath the waves. Bone and antler points from North Sea Doggerland off the Dutch coast, in: Groß, D., Lübke, H., Meadows, J., Jantzen, D. (Eds.), Working at the Sharp End: From Bone and Antler to Early Mesolithic Life in Northern Europe. Untersuchungen Und Materialien Zur Steinzeit in Schleswig-Holstein Und Im Ostseeraum 10. Wachholtz Verlag, Kiel/Hamburg, pp. 383–404. https://doi.org/10.23797/9783529018619-16.

Aveling, E.M., Heron, C., 1999. Chewing tar in the early Holocene: An archaeological and ethnographic evaluation. Antiquity 73, 579–584. https://doi.org/10.1017/S0003598X00065133.

Bigga, G., Schoch, W.H., Urban, B., 2014. Paleoenvironment and possibilities of plant exploitation in the Middle Pleistocene of Schöningen (Germany). Insights from botanical macro-remains and pollen. J. Hum. Evol. 89, 92–104. https://doi.org/10.1016/J.JHEVOL.2015.10.005.

Boëda, E., Bonilauri, S., Connan, J., Jarvie, D., Mercier, N., Tobey, M., Valladas, H., al Sakhel, H., Muhesen, S., 2008. Middle Palaeolithic bitumen use at Umm el Tlel around 70 000 BP. Antiquity 82, 853–861. https://doi.org/10.1017/S0003598X00097623.

Chapters, S., Evershed, R.P., Goad, L.J., Heron, C., Blinkhorn, P., 1993. Identification of an adhesive used to repair a Roman jar. Archaeometry 35, 91–101. https://doi.org/10.1111/j.1475-4754.1993.tb01025.x.

Charrié-Duhaut, A., Porraz, G., Cartwright, C.R., Igreja, M., Connan, J., Poggenpoel, C., Texier, P., 2013. First molecular identification of a hafting adhesive in the Late Howiesons Poort at Diepkloof Rock Shelter (Western Cape, South Africa). J. Archaeol. Sci. 40, 3506–3518. https://doi.org/10.1016/j.jas.2012.12.026.

Cîntă-Pînzaru, S., Dehelean, C.A., Soica, C., Culea, M., Borcan, F., 2012. Evaluation and differentiation of the Betulaceae birch bark species and their bioactive triterpene content using analytical FT-vibrational spectroscopy and GC-MS. Chem. Cent. J. 6, 67. https://doi.org/10.1186/1752-153X-6-67.

Colombini, M.P., Giachi, G., Modugno, F., Ribechini, E., 2005. Characterisation of organic residues in pottery vessels of the Roman age from Antinoe (Egypt). Microchem. J. 79, 83–90. https://doi.org/10.1016/J.MICROC.2004.05.004.

Connan, J., Van de Velde, T., 2010. An overview of bitumen trade in the Near East from the Neolithic (c.8000 BC) to the early Islamic period. Arab. Archaeol. Epigr. 21, 1–19. https://doi.org/10.1111/J.1600-0471.2009.00321.X.

Courel, B., Schaeffer, P., Féliu, C., Thomas, Y., Adam, P., 2018. Birch bark tar and jewellery: The case study of a necklace from the Iron Age (Eckwersheim, NE France). J. Archaeol. Sci. Reports 20, 72–79. https://doi.org/10.1016/j.jasrep.2018.04.016.

Degano, I., Soriano, S., Villa, P., Pollarolo, L., Lucejko, J.J., Jacobs, Z., Douka, K., Vitagliano, S., Tozzi, C., 2019. Hafting of Middle Paleolithic tools in Latium (central Italy): New data from Fossellone and Sant'Agostino caves. PLoS One 14. https://doi.org/10.1371/journal.pone.0213473.

Dinnis, R., Pawlik, A., Gaillard, C., 2009. Bladelet cores as weapon tips? Hafting residue identification and micro-wear analysis of three carinated burins from the late Aurignacian of Les Vachons, France. J. Archaeol. Sci. 36, 1922–1934. https://doi.org/10.1016/j.jas.2009.04.020.

Edwards, H.G.M., Farwell, D.W., Daffner, L., 1996. Fourier-transform Raman spectroscopic study of natural waxes and resins. I. Spectrochim Acta Part A Mol. Biomol. Spectrosc. 52, 1639–1648. https://doi.org/10.1016/0584-8539(96)01730-8.

Fajardo, S., Kozowyk, P.R.B., Langejans, G.H.J., 2023. Measuring ancient technological complexity and its cognitive implications using Petri nets. Sci. Rep. 13, 14961. https://doi.org/10.1038/s41598-023-42078-1.

Font, J., Salvadó, N., Butí, S., Enrich, J., 2007. Fourier transform infrared spectroscopy as a suitable technique in the study of the materials used in waterproofing of archaeological amphorae. Anal. Chim. Acta 598, 119–127. https://doi.org/10.1016/J.ACA.2007.07.021.

Heron, C., Evershed, R.P., 1993. The analysis of organic residues and the study of pottery use. Archaeol. Method Theory 5, 247–284.

Kozowyk, P.R.B., Langejans, G.H.J., Poulis, J.A., 2016. Lap shear and impact testing of ochre and beeswax in experimental Middle Stone Age compound adhesives. PLoS One. https://doi.org/10.1371/journal.pone.0150436.

Kozowyk, P.R.B., Poulis, J.A., Langejans, G.H.J., 2017. Laboratory strength testing of pine wood and birch bark adhesives: a first study of the material properties of pitch. J. Archaeol. Sci. Reports 13, 49–59. https://doi.org/10.1016/j.jasrep.2017.03.006.

Kozowyk, P.R.B., van Gijn, A.L., Langejans, G.H.J., 2020. Understanding preservation and identification biases of ancient adhesives through experimentation. Archaeol. Anthropol. Sci. 12, 1–17. https://doi.org/10.1007/s12520-020-01179-y.

Kristiansen, K., Suchowska-Ducke, P., 2022. Connected histories: The dynamics of Bronze Age interaction and trade 1500–1100 BC. Proc. Prehist. Soc 81, 361–392. https://doi.org/10.1017/ppr.2015.17.

Langejans, G., Aleo, A., Fajardo, S., Kozowyk, P., 2022. Archaeological adhesives. Oxford Res. Encycl. Anthropol. https://doi.org/10.1093/acrefore/9780190854584.013.198.

Langejans, G.H.J., Pomstra, D., Ducrocq, T., Haskins, A., Kozowyk, P.R.B., 2024. Conifer tar in the late Upper Palaeolithic and Mesolithic of north-western Europe. Analecta Praehist. 52, 45–62.

Martín-Ramos, P., Fernández-Coppel, I.A., Ruíz-Potosme, N.M., Martín-Gil, J., 2018. Potential of ATR-FTIR spectroscopy for the classification of natural resins. Biol. Eng. Med. Sci. Reports 4, 03–06. https://doi.org/10.5530/bems.4.1.2.

Mazza, P.P.A., Martini, F., Sala, B., Magi, M., Colombini, M.P., Giachi, G., Landucci, F., Lemorini, C., Modugno, F., Ribechini, E., 2006. A new palaeolithic discovery: Tar-hafted stone tools in a European Mid-Pleistocene bone-bearing bed. J. Archaeol. Sci. 33, 1310–1318. https://doi.org/10.1016/j.jas.2006.01.006.

Mitikidou, S., Dimitrakoudi, E., Urem-Kotsou, D., Papadopoulou, D., Kotsakis, K., Stratis, J.A., Stephanidou-Stephanatou, I., 2008. Organic residue analysis of Neolithic pottery from North Greece. Microchim. Acta 160, 493–498. https://doi.org/10.1007/s00604-007-0811-2.

Monnier, G.F., Hauck, T.C., Feinberg, J.M., Luo, B., Le Tensorer, J.-M., al Sakhel, H., 2013. A multi-analytical methodology of lithic residue analysis applied to paleolithic tools from Hummal, Syria. J. Archaeol. Sci. 40, 3722–3739. https://doi.org/10.1016/j.jas.2013.03.018.

Monnier, G., 2017. University of Minnesota archaeological materials infrared spectra library [WWW Document]. URL https://ftir.elevator.umn.edu/page/view/11 (accessed 9.28.21).

Odegaard, N., Pool, M., Bisulca, C., Santarelli, B., Neiman, M., Watkinson, G., 2014. Pine Pitch: New treatment protocols for a brittle and crumbly conservation problem. Objects Spec. Gr. Postprints 21, 21–41.

Ominami, Y., 2018. Environmental SEM (atmospheric SEM), in: The Surface Science Society of Japan (Ed.), Compendium of Surface and Interface Analysis. Springer, Singapore, pp. 165–169. https://doi.org/10.1007/978-981-10-6156-1_28.

Pawlik, A.F., Thissen, J., 2011. The 'Palaeolithic prospection in the Inde Valley' project. E&G Quat. Sci. J. 60, 66–77. https://doi.org/10.3285/eg.60.1.04.

Pawlik, A.F., 2004. Identification of hafting traces and residues by scanning electron microscopy and energy-dispersive analysis of X-rays, in: Walker, E.A., Wenban-Smith, F., Healy, F. (Eds.), Lithics in Action. Oxbow Books, Oxford, pp. 169–179.

Rageot, M., Pêche-Quilichini, K., Py, V., Filippi, J., Fernandez, X., Regert, M., 2016. Exploitation of beehive products, plant exudates and tars in Corsica during the Early Iron Age. Archaeometry 58, 315–332. https://doi.org/10.1111/arcm.12172.

Rageot, M., Théry-Parisot, I., Beyries, S., Lepère, C., Carré, A., Mazuy, A., Filippi, J.J., Fernandez, X., Binder, D., Regert, M., 2019. Birch bark tar production: Experimental and biomolecular approaches to the study of a common and widely used prehistoric adhesive. J. Archaeol. Method Theory 26, 276–312. https://doi.org/10.1007/s10816-018-9372-4.

Rageot, M., Lepère, C., Henry, A., Binder, D., Davtian, G., Filippi, J., Fernandez, X., Guilaine, J., Jallet, F., Radi, G., Thirault, E., Terradas, X., Regert, M., 2021. Management systems of adhesive materials throughout the Neolithic in the North-West Mediterranean. J. Archaeol. Sci. 126 (10530), 105309 https://doi.org/10.1016/j.jas.2020.105309.

Regert, M., 2004. Investigating the history of prehistoric glues by gas chromatography-mass spectrometry. J. Sep. Sci. 27, 244–254. https://doi.org/10.1002/jssc.200301608.

Regert, M., Garnier, N., Decavallas, O., Cren-Olive, C., Rolando, C., 2003. Structural characterization of lipid constituents from natural substances preserved in archaeological environments. Meas. Sci. Technol. 14, 1620–1630. https://doi.org/10.1088/0957-0233/14/9/313.

Ribechini, E., Orsini, S., Silvano, F., Colombini, M.P., 2009. Py-GC/MS, GC/MS and FTIR investigations on LATE Roman-Egyptian adhesives from opus sectile: New insights

into ancient recipes and technologies. Anal. Chim. Acta 638, 79–87. https://doi.org/10.1016/J.ACA.2009.02.004.
Schippers, A., Jorgensen, B.B., 2002. Biogeochemistry of pyrite and iron sulfide oxidation in marine sediments. Geochim. Cosmochim. Acta 66, 85–92. https://doi.org/10.1016/S0016-7037(01)00745-1.
Urem-Kotsou, D., Stern, B., Heron, C., Kotsakis, K., 2002. Birch-bark tar at Neolithic Makriyalos, Greece. Antiquity 76, 962–967. https://doi.org/10.1017/S0003598X00091766.
Vahur, S., Teearu, A., Peets, P., Joosu, L., Leito, I., 2016. ATR-FT-IR spectral collection of conservation materials in the extended region of 4000–80 cm–1. Anal. Bioanal. Chem. 408, 3373–3379. https://doi.org/10.1007/s00216-016-9411-5.
Wadley, L., Williamson, B., Lombard, M., 2004. Ochre in hafting in Middle Stone Age southern Africa: a practical role. Antiquity 78 (301), 661–675. https://doi.org/10.1017/S0003598X00113298.
Weiner, S., 2010. Infrared spectroscopy in archaeology, in: Microarchaeology: Beyond the Visible Archaeological Record. Cambridge University Press, Cambridge, pp. 275–316. https://doi.org/https://doi.org/10.1017/CBO9780511811210.013.
Wragg Sykes, R.M., 2015. To see a world in a hafted tool: Birch pitch composite technology, cognition and memory in Neanderthals, in: Coward, F., Hosfield, R., Pope, M., Wenban-Smith, F. (Eds.), Settlement, Society and Cognition in Human Evolution: Landscapes in Mind. Cambridge University Press, Cambridge, pp. 117–137. https://doi.org/10.1017/CBO9781139208697.008.